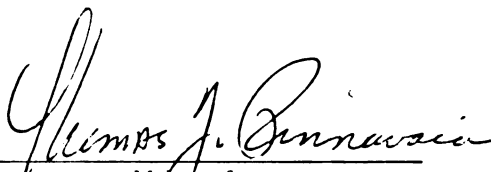This is to certify that the

dissertation entitled

Synthesis, Characterization and Catalytic Properties of a
New Family of Tubular Silicate-Layered Silicate
Intercalation Complexes

presented by

Todd Allen Werpy

has been accepted towards fulfillment
of the requirements for

___Ph.D.___ degree in ___Chemistry___

_____
Major professor

Date _/-22-91_____

PLACE IN RETURN BOX to remove this checkout from your record.
TO AVOID FINES return on or before date due.

DATE DUE	DATE DUE	DATE DUE
SEP 2 6 ... FEB 3 0 ...		

MSU Is An Affirmative Action/Equal Opportunity Institution

c:\circ\datedue.pm3-p.1

SYNTHESIS, CHARACTERIZATION AND CATALYTIC PROPERTIES OF A

NEW FAMILY OF TUBULAR SILICATE-LAYERED SILICATE

INTERCALATION COMPLEXES

By

Todd Allen Werpy

A DISSERTATION

Submitted to

Michigan State University

in partial fulfillment of the requirements

for the degree of

DOCTOR OF PHILOSOPHY

Department of Chemistry

1991

ABSTRACT

SYNTHESIS, CHARACTERIZATION AND CATALYTIC PROPERTIES OF A NEW FAMILY OF TUBULAR SILICATE-LAYERED SILICATE INTERCALATION COMPLEXES

By

Todd Allen Werpy

This dissertation describes the synthesis, characterization and catalytic activity of a novel family of pillared clays in which the pillar is a nanotubular aluminosilicate known as imogolite. This new family of pillared clays differs from those previously prepared in that the pillar itself offers intrinsic microporosity as opposed to the microporosity being generated by lateral separation between the pillars. The reaction of Na^+-montmorillonite with imogolite at a pH of 6.5 leads to the formation of a new family of pillared clays characterized by a 33Å lattice expansion, as well as by thermal stabilities above 400°C. These new nanocomposite materials also show surface areas of greater than 300 m^2/g and microporous pore volumes of 0.10 cm^3/g as well as a total liquid pore volume of 0.16 cm^3/g. MAS-NMR results indicate that the intercalation of the imogolite into the host clay has little or no effect upon the chemical constitution of the imogolite tubes and, in fact, stabilizes the tubes from collapse as evidenced by differential thermal analysis. Pristine imogolite tubes showed almost a total loss in surface area at temperatures above 250°C while the imogolite pillared

montmorillonite retained essentially all of its surface area at temperatures above 400°C.

Montmorillonite and beidellite both served as host clays for the intercalation of imogolite. This new family of tubular silicate-layered silicate (TSLS) intercalation complexes posses both Bronsted and Lewis acidity. The beidellite-imogolite complex showed much higher Bronsted acidity than the montmorillonite-imogolite complex, as evidenced by FTIR results obtained from pyridine adsorption. Cumene cracking has been used as a model reaction for elucidating the Bronsted acidity of these materials. The TSLS montmorillonite complex showed an initial cumene conversion at 350°C of 55 % while the TSLS beidellite showed an initial cumene conversion of almost 90 %. Shape selectivity was determined by the isomerization of m-xylene to o-xylene and p-xylene. The TSLS beidellite complex showed a 90 % selectivity to isomerized products while the TSLS montmorillonite showed only a 50 % selectivity to isomerized products. These selectivities are consistent with the microporous nature of the TSLS intercalation compounds.

To My Family

ACKNOWLEDGEMENTS

I would like to thank Dr. Thomas Pinnavaia for his patients and guidance which he so willingly gave throughout the course of this endeavor. I hope that after my graduation our relationship will continue to grow both personally and professionally.

I would also like to thank the other members of my committee, Dr. Dan Nocera, Dr. John Stille and Dr. Dennis Miller who dedicated their time and effort in helping edit this dissertation.

I would also like to thank the Department of Chemistry at Michigan State University for giving me the opportunity to undertake this study. I would also like to thank the support personnel who made my stay here much more enjoyable.

Finally, I would like to thank my past and present group members for making this experience a truly memorable one.

TABLE OF CONTENTS

LIST OF TABLES

LIST OF FIGURES

CHAPTER I

General Introduction

To Pillared Clays and Imogolite

1.1. Pillared Clays

Pillared clays are smectite silicates in which the naturally occurring interlayer cation has been replaced through ion exchange by a robust cation which acts a molecular prop. These molecular props allow for the permanent expansion of the layers of the host clay. In such cases there is no need for a solvent to be present in order for the layers to remain separated[1]. In addition, the lateral separation of the pillaring agent intoduces permanent porosity and allows access of guest molecules in the interlayer space or "galleries" of the host clay. Various types of cations have been used as pillaring agents such as alkylammonium ions[2], bicyclic amines[3], and polynuclear hydroxy metal cations[4]. Figure I.1 is a schematic representation of a pillared clay and illustrates the various pillaring agents used[1].

The concept of pillared clays was demonstrated more than 25 years ago by Barrer and McLeod[5]. They showed that permanent porosity could be introduced into montmorillonite by replacing the interlayer alkali metal with tetraalkylammonium ions. They were able to further

demonstrate that these new pillared clays showed selective adsorption and could be thought of as two dimensional zeolites. These materials did not receive as much attention as they deserved because of progress being made in the synthesis and catalytic properties of zeolites. Pillared clays are now receiving renewed interest as catalysts because of the development of pillars which allow the pore sizes to be larger than that of faujasitic zeolites. In addition, the pore sizes are somewhat tuneable by varying the size of the pillaring agent which changes the layer separation. Different pore sizes can also be achieved by modifying the charge on the pillar which affects the lateral separation between the pillars. The fact that pillared clays have adjustable pore sizes and that these pore sizes can be quite large makes these materials especially inviting for the catalysis of larger molecules such as the cracking of oil[1].

A second fundamental reason that pillared clays have enjoyed renewed enthusiasm is due to the increased thermal stability of metal cation pillars. The pillaring agents illustrated in Figure I.1 have very different thermal stabilities. The alkylammonium and bicyclic amines tend to decompose below 250°C and metal chelates below 450°C[6]. Stability to temperatures in excess of 500°C have been obtained for metal oxide pillared clays[7-10] by Brindley and others. They also reported the successful synthesis of hydroxy aluminum and hydroxy zirconium cations by base

Molecular props

$M_x(OH)_y^{n+}$

$M(chel)_3^{n+}$
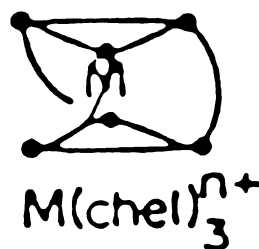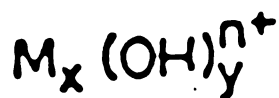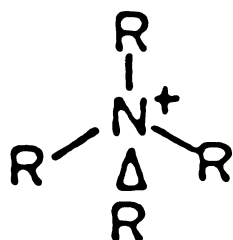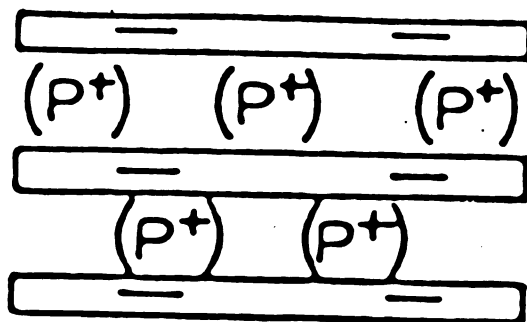
Figure I.1 Schematic representation of a pillared clay showing the required lateral separation of the pillars and a variety of pillaring agents.

hydrolysis which yielded thermally stable (>500°C) pillared clays with surface areas between 200 and 500m^2/g.

The hydroxy zirconium pillaring agent contains cations of the type $Zr_4(OH)^{x+}_{16-x}$[11]. The hydroxy aluminum was first suggested to be an Al_6 oligomer[7]; however, the structure of the pillaring cation is most likely based on an Al_{13} oligomer related to the known cation $Al_{13}O_4(OH)_{24}^{7+}$[12]. This structure has also been reconfirmed by ^{27}Al NMR and potentiometric titration data[1].

A metal oxide cluster is generated by the dehydroxylation of the hydroxy cation after intercalation into the host clay. In the case of Al_{13}-montmorillonite the formation of the metal oxide may be shown as follows:

$$Al_{13}O_4(OH)_{28+n}^{(3-n)+} \quad \xrightarrow{-H_2O} \quad 6.5\ Al_2O_3 + (3-n)H^+$$
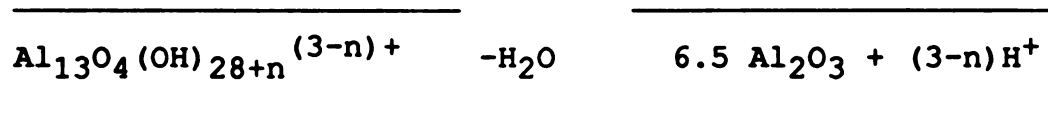
where the aluminum is in small clusters. The exact location of the protons in the intercalation complex is still not certain[1].

The oxometal species capable of forming pillared clays depends upon the hydrolysis chemistry of the polyoxo cation precursor. The properties of the resulting pillared clays also are dependent on this same hydrolysis chemistry[13].

1.2 Objectives of Dissertation Research

The objective of this dissertation is to examine the synthesis, physical properties, and catalytic activity of a new type of pillared clay. This new family of pillared clays results from the intercalation of a regular tubular aluminosilicate known as imogolite into the galleries of various smectite clays. This new family constitutes a new synthesis direction that involves direct intercalation of metal oxide sol particles into the host clay galleries. The typical synthesis of pillared clays previously focussed on the intercalation of a polyoxocation followed by calcination to the metal oxide. This new strategy will involve the direct intercalation of molecular-size aluminosilicates. The effect of this type of synthesis on the physical and catalytic properties of these new pillared clays will be discussed.

1.3 Structure of Smectite Clay Minerals

The term "clay" refers to a finely divided mineral with a particle size of less than two microns. The term "clay mineral" refers to silicate clays with definite stoichiometry and crystalline structure[14]. Figure I.2 illustrates schematically the idealized structure of a smectite clay mineral layer. The oxygen atoms define upper and lower sheets of tetrahedral sites and a central sheet of octahedral sites. The relationship between the two tetrahedral sheets and the one octahedral sheet within a

$$M^{n+} \cdot xH_2O$$
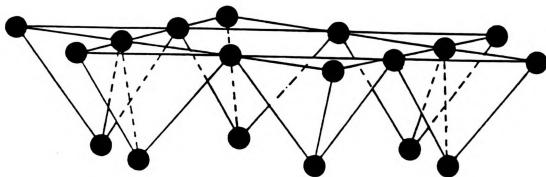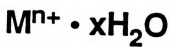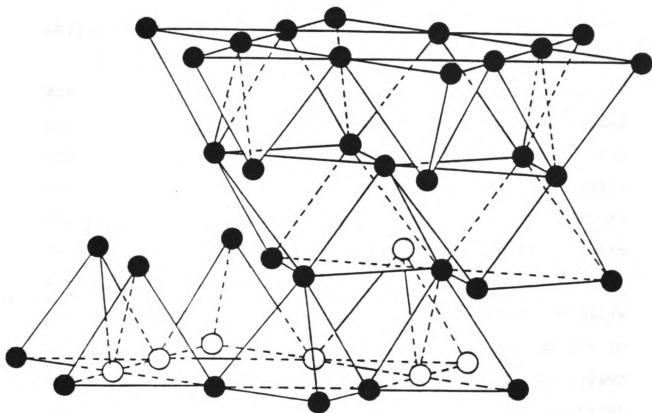
Figure I.2   Idealized structure of a smectite clay mineral
layer.

layer defines the smectite clay as being a member of the 2:1 phyllosilicates structure type.

The two tetrahedral sheets condensed to an octahedral sheet define a clay layer. The distance between the top of one layer and the top of an adjacent layer, which encompass the thickness of the clay layer and the height of the interlayer gallery, is defined as the basal spacing. Basal spacings are defined by the d(001) reflections, which can readily be measured by X-ray diffraction of oriented film samples.

The different members of the smectite group of clays are distinguished by the type and location of the cations in the oxygen framework. A unit cell consists of 20 oxygen atoms and 4 hydroxyl groups. These 24 lacttice positions describe eight tetrahedral and six octahedral intersticies for occupancy by metal cations. When two-thirds of the octahedral sites are occupied by cations, the clay is classified as a dioctahedral 2:1 phyllosilicates. If all of the octahedral sites are occupied by cations, the clay is labelled as being a trioctahedral 2:1 phyllosilicate. Table I.1 lists the idealized structural formulas for various dioctahedral and trioctahedral smectites. Included for comparison are the structural formulas for two micas (muscovite and phlogopite), pyrophyllite and talc[15].

The structure of a smectite has a framework negative charge of 44. To balance this negative charge, cations occupy the octahedral and tetrahedral sites. Obviously,

Table I.1 Idealized structural formulas for some 2:1
clay minerals.

Dioctahedral

Pyrophyllite: $[Al_{4.0}](Si_{8.0})O_{20}(OH)_4$

Montmorillonite: $M_{x/n}^{n+} \cdot yH_2O[Al_{4.0-x}Mg_x](Si_{8.0})O_{20}(OH)_4$

Beidellite: $M_{x/n}^{n+} \cdot yH_2O[Al_{4.0}](Si_{8.0-x}Al_x)O_{20}(OH)_4$

Nontronite: $M_{x/n}^{n+} \cdot yH_2O[Fe_{4.0}](Si_{8.0-x}Al_x)O_{20}(OH)_4$

Muscovite: $K_2[Al_{4.0}](Si_{6.0}Al_{2.0})O_{20}(OH)_4$

Trioctahedral

Talc: $[Mg_{6.0}](Si_{8.0})O_{20}(OH)_4$

Hectorite: $M_{x/n}^{n+} \cdot yH_2O[Mg_{6.0-x}Li_x](Si_{8.0})O_{20}(OH,F)_4$*

Saponite: $M_{x/n}^{n+} \cdot yH_2O[Mg_{6.0}](Si_{8.0-x}Al_x)O_{20}(OH)_4$

Phlogopite: $K_2[Mg_{6.0}](Si_{6.0}Al_{2.0})O_{20}(OH)_4$

differently charged cations could be used to balance this negative charge. In the case of talc all of the tetrahedral sites are occupied by Si(IV), while all of the octahedral sites are occupied by Mg(II). This type of occupancy leads to a neutral trioctahedral layer. Neutral 2:1 structure types are of little value in the synthesis of pillared clays. Dioctaherdral pyrophyllite achieves its electrical neutrality from the presence of Si(IV) in all eight tetrahedral holes and Al(III) in two-thirds of the octahedral holes. The micas, muscovite and phlogopite have vastly different charges due to the substitution of Si(IV) by Al(III) in the tetrahedral positions. This substitution results in a net negative charge of $2e^-$ per Si_8O_{20} unit which is balanced by potassium ions in the interlayer. These interlayer potassium ions coordinate to the hexagonal arrays of oxygen atoms at the layer surface.

The charge on the layers of smectites falls between talc and muscovite. The negative charge ranges from $0.4e^-$ to $1.2e^-$ per Si_8O_{20} unit. To balance the layer charge, layers of hydrated cations are intercalated between the silicate layers. Generally, these intercalated cations are alkaline earth ions such as Ca(II) or alkali earth metals like Na(I)[2]. Because of the intermediate charge on the smectite clay minerals they are very attractive as hosts for various other cations.

1.4 Swelling Properties of Smectites

The hydration sphere associated with the interlayer cation depends in part on the hydration energy of the cation. Depending on the amount of water contained in the interlayer galleries, the water may be ordered or highly disordered (solution-like) in the interlamellar region. The extent of interlayer swelling in clays can be measured by X-ray diffraction.

The basal spacing of dehydrated Na^+-montmorillonite is 9.5Å. As the water content increases, spacings of 12.4, 15.4 and 18.6Å are observed. These increased spacings correspond to one, two, or three layers of water associated with the Na(I) ion, respectively. Further swelling can occur when Na^+-montmorillonite is suspended in water. In fact, the aluminosilicate layers can become completely dispersed with the interlayer spacing being essentially infinite.

Increasing the concentration of clay suspensions can cause gelation. This gelation phenomenon results from extensive edge-to-face and edge-to-edge layer interactions generating a "house of cards" structure[15]. This swelling phenomenon allows for the identification of certain classes of clays. The ability of clays to swell in also critical to the design of clay intercalates. If clays did not swell it would be difficult to exchange one gallery cation for another.

1.5 Ion Exchange in the Interlayer

Interlayer cations can be replaced through ion exchange reactions with other cations, such as organic ions[14], metal complexes[16], silicates[17], or polyoxo-inorganic cations[1]. Several of these are robust cations that act as pillars and prop the clay layer apart without requiring the presence of a solvent. Ion exchange reactions in clay minerals have several characteristics in common[6]. Reaction rates are controlled by diffusion of the ion into the interlayer. This process occurs as the exchanging ions move against a concentration gradient. The higher the concentration gradient, the faster the exchange rate will be. The second common characteristic is that the exchange is stoichiometric with respect to conservation of charge. Finally, ion exchange reactions are ion selective. Among monovalent cations, the smaller the effective radius, the more preferred is the binding. The ability of clays to undergo ion exchange is the fundamental principle behind the synthesis of new pillared materials.

1.6 Acidity

Hydrated cations in smectite clay galleries contribute to the acidic nature of pillared clays. The water molecules in the primary hydration sphere are polarized and partly dissociated. This is illustrated schematically below:

$$Na^+(H_2O)_x \qquad\qquad Na(OH)_{x-1} + H_2O$$
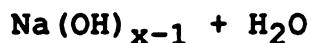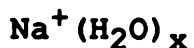
The Bronsted acidity of hydrated cations in the clay galleries can be greater than that of the same cation in aqueous solution[18]. The acidity can be correlated with the cation polarizing power which increases with increasing charge-to-radius ratio. In addition, the acidity increases as the amount of interlamellar water decreases. Lewis acidity is also intrinsically present in smectites clays.

1.7 Catalysis

The use of heterogeneous catalysts in commercially viable processes for the conversion of raw organic chemicals to useful products is becoming increasingly more important. As raw materials become less available and of poorer quality the need to develop new catalysts with higher conversions and greater selectivity to desired products will become essential to the chemical industry. At the present time, zeolites represent the largest volume of commercial catalysts in use for the conversion of raw organic chemicals to useful products. Zeolites offer not only significant catalytic activity because of the strong Bronsted acidity but also offer a high degree of selectivity because of the unique pore structures.

Several different organic conversions have been used to characterize the effectiveness of zeolites as acid

catalysts[19]. The two most important features in selecting control reactions are conversion and selectivity to desired products. The most common of these reactions is the cracking of cumene to benzene and propylene[20]. This reaction is useful because it tends to give only two products and gives insight into the availability of Bronsted acid sites on the catalyst. It is not particularly useful however in yielding information of selectivity. Another common reaction which helps elucidate the acidity of a catalyst is the conversion of n-decane to paraffins and olefins[20]. This reaction yields information on both the strength of the acid sites and on pore size and catalyst shape depending on the chain length and isomerization products obtained by the reaction. The reaction schemes for these two conversions is given in Figure I.3.

In addition to the importance of acidity there is also a need to be concerned about selectivity. A good catalyst would not only show acceptable conversion levels, but would also be selective to useful products. Selectivity can generally be broken down into three different classes. Reactant selectivity, where only reactants with a specific size range can reach the active sites in the catalyst. Product selectivity happens when only products that have been generated in the porous structure have the correct molecular dimensions to diffuse out of the pores. The final selective possibility is transition state selectivity. This occurs when only certain intermediates are allowed to form
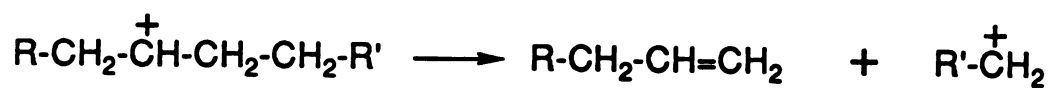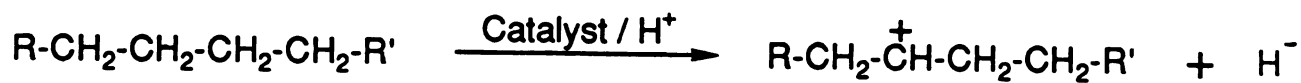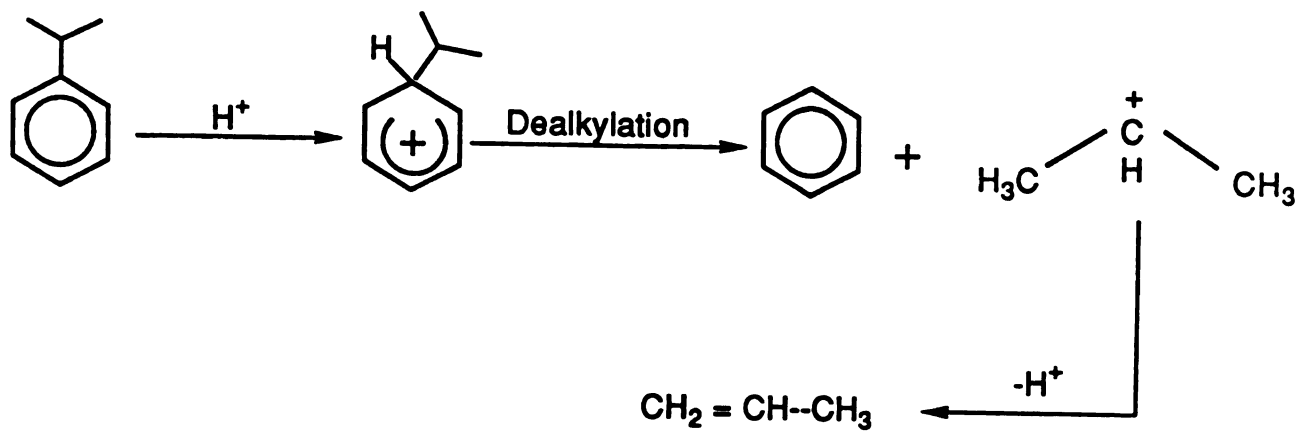
Figure I.3 Reaction schemes for the catalytic cracking of cumene and of parrafins.

in the pores of the catalyst while those intermediates with molecular dimensions that are to large to fit in the pores are not allowed to form. This type of selectivity is the most difficult to prove because many of the intermediates are not well defined[18].

Another reaction that is useful in evaluating shape selectivity is the isomerization of meta-xylene. In this reaction the substrate can undergo either isomerization to ortho-xylene or para-xylene or disproportionation to toluene and various trimethyl benzenes. The selectivity is then defined by the %isomerization divided by the %isomerization plus the %disproportionation. The reaction schemes for these conversions are given in Figure I.4.

Use of the above reactions can provide insight into both the acidity and selectivity of catalysts which are intended to be used in the conversion of organic reactants.

1.8 Pillared Clays as Catalysts

The majority of the work involving pillared clays as catalysts has been devoted to aluminum pillared clays, in particular, alumina pillared montmorillonite. The structure of the pillaring cation used to form an alumina pillar is given in Figure I.5.

The synthesis of aluminum pillared clay requires the intercalation of $Al_{13}O_4(OH)_{24}^{7+}$ [7] by ion exchange, with the Na^+ form of the host clay. This material is then calcined to form Al_2O_3 particles between the layers of the clay host.
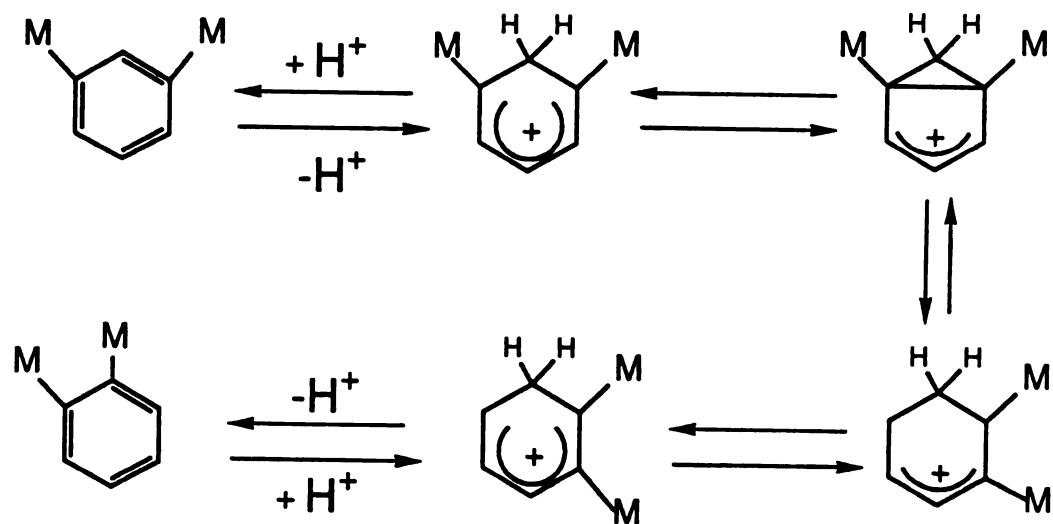
Figure I.4   Reaction scheme for the isomerization of m-xylene to ortho and para xylene.

$$[Al_{13}O_4(OH)_{24}(H_2O)_{12}]^{7+}$$
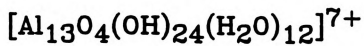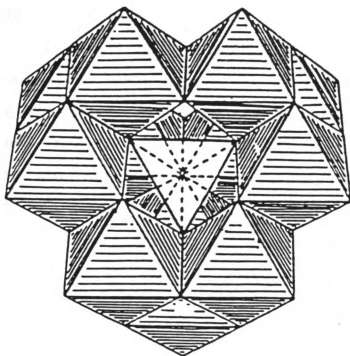
Figure I.5   Schematic representation of the Al_{13} polyoxo-
cation pillar.

Upon calcination, dehydroxylation of the Al_{13} polyoxocations occurs. This material is then considered to be pillared in as much as the layers are permanently expanded and a permanent microporosity has been introduced into the aluminum pillared smectite. These materials have been shown by several workers[10,11,19] to be reasonably good acid catalysts. One possible reason for the improved Bronsted acidity of the aluminum pillared smectites is that protons are generated during dehydroxylation. The activity of these materials are somewhat less than comparable zeolites but not unworthy of further study. The major drawback to these materials is that they show limited selectivity. This limited selectivity in certain reactions is due to the large pore volumes associated with these materials.

1.9 Direct Intercalation of Metal Oxides (DIMOS)

Several workers have recognized the possibility of directly intercalating metal oxide sol particles into clay galleries[21-24]. The advantage of using this method of direct intercalation would be the elimination of the calcination procedure which is required for metal oxide pillared clays. The intrinsic problem in the process however, is finding sol particles which are very uniform in size. Although commercial sols are available, it is difficult to obtain a monodispersed solution of the particles in the molecular size range (<50Å). In addition,

these sols tend to be uniform within only a few angstroms.

1.10 Imogolite

A naturally occurring tubular metal oxide known has imogolite[25-28] has the potential to overcome these limitations associated with commercial sols. Imogolite is found not only in nature, but is can also be made synthetically.

The name and structure of imogolite was first introduced in 1962 by Yoshinga and Aomine[25]. With only limited data available on imogolite, the initial result they reported was that imogolite was a compound with the derived chemical formula $1.5SiO_2 \cdot Al_2O_3 \cdot 2.5H_2O$. In 1966 Wada was able to elaborate on the structure of imogolite by obtaining a relatively pure sample. The infrared spectrum suggested a unique structure, and chemical analysis verified the presence of an oxide consisting of only SiO_2, Al_2O_3, and H_2O. Deuterium exchange showed the presence surface hydroxyl groups. In 1967 Wada proposed that imogolite was simply an end member of allophane and actually had a chemical composition ranging from $SiO_2 \cdot Al_2O_3.3H_2O$ to $2SiO_2 \cdot Al_2O_3 \cdot 3H_2O$. In 1969 Russel et al.[26] used infrared and electron diffraction to support the structure of imogolite. The use of electron diffraction unambiguously showed that imogolite consisted of fibers with 8.4Å repeat units parallel to the fiber axis and 23Å perpendicular to it. These parameters could not be satisfied by the

structure proposed by Wada in 1967. The use of infrared showed an adsorption band near $930cm^{-1}$ which could be interpreted in terms of the presence of Si_2O_7 units. Based on this evidence Russel et al.[29] proposed a layered chain structure for imogolite. However, in 1972 Cradwick, Farmer, and Russel proposed that imogolite was a hydrated aluminosilicate of tubular structure[30]. The structure is illustrated in Figure I.6.

The resulting idealized chemical formula for imogolite was $SiO_2Al_2O_32H_2O$, in very good agreement with the experimental formula of $1.1SiO_2Al_2O_32.5H_2O$. The structure of imogolite can be viewed as a gibbsite sheet in which orthosilicate groups have condensed in the inner hydroxyl plane at triangular faces above vacant octahedral positions. When this condensation reaction occurs, there is a shortening of the SiOAl bond, causing the sheet to curl. The sheet then curls to the point where it condenses onto itself and forms a tube. The requirement for the completion of the imogolite tube is that there can only be 12 edge shared octahedral linked together in synthetic imogolite. Naturally occurring imogolite is somewhat smaller and interestingly requires only 11 edge shared octahedral. The final imogolite has a diameter of 23Å for synthetic imogolite and 21Å for naturally occurring imogolite. This is now the accepted structure for imogolite and has been confirmed by MAS-NMR[31].

The first successful synthesis of imogolite in the

laboratory was performed by Farmer in 1981[31]. Farmer synthesized imogolite by the digestion of hydroxy aluminum complexes formed at a pH of 3.2 to 5.5 in aqueous solutions with aluminum concentrations of less than 5.0mmole per liter and silicon concentrations of less than 3.0 mmole per liter. To compare the structure of synthetic imogolite to natural imogolite, Farmer used electron microscopy, electron diffraction, and infrared spectroscopy. The only difference that appeared was that synthetic imogolite was 10 to 15 percent larger than natural imogolite as was expected for 12 repeat units along the circumference of the tube[29].

1.11 Physical Properties of Imogolite

The X-ray diffraction pattern of imogolite consists of several broad reflections. These reflections occur at 12-20,7.8-8.0, and 5.5-5.6Å[28]. The X-ray diffraction pattern along with the changes that occur upon heating serve as a good criterion for distinguishing imogolite from other clay minerals, since there are very few similarities with these minerals.

Thermal analysis is also a useful tool for characterizing imogolite. Imogolite gives a large endothermic peak between 50-300°C on the DTA curve due to a loss of a large amount of adsorbed water. Imogolite also gives an exothermic peak at 390-420°C from dehydroxylation. The appearance of an endothermic peak at 900-1100°C is caused by imogolite changing to mullite. On the TGA curve

there is a continuous weight loss from 25°C to 300°C. This weight loss accounts for about 30% of the total mass of imogolite. At 300°C there is a more abrupt weight loss of about 10% from dehydroxylation[33].

Infrared spectroscopy shows major broad adsorption bands in three regions, 2800-3000cm^{-1}, 1400-1800cm^{-1}, and 650-1200cm^{-1}. The stretching frequency in the region 2800-3800cm^{-1} is attributed to OH stretching of adsorbed H_2O or surface OH groups. An adsorption band due to the HOH deformation vibration occurs around 1630-1640cm^{-1}. Imogolite also shows an adsorption band at 930cm^{-1} due to the SI-O stretch from the SiO_3OH group[29].

Electron diffraction of imogolite gave a series of ring reflections at 1.4, 2.1, 2.3(broad),3.3(broad),3.7, 4.1, 5.7(broad), 11.8(broad), and 21-23Å[26-28]. The 1.4 and 2.1Å reflections were interpreted as higher order reflections arising from a repeat unit of 8.4Å along the tube axis. The 5.7, 7.8, and 11.8Å reflections were interpreted as higher order reflections due to the 21-23Å interaxial separations of the tube unit[30].

The BET surface area of imogolite was reported to be 140 m^2/g by N_2 adsorption. This was determined by using a freeze dried sample of imogolite[29].

1.12 Chemical Properties of Imogolite

Cation exchange capacity values for natural imogolite have been hard to establish due to impurities in the soil samples. The best results were obtained by equilibrating imogolite with 0.05N Na[CH$_3$COO] at a pH of 7.0. The resulting value was 30 meq/100g. The cation exchange capacity of imogolite comes from the dissociation of surface hydroxyl groups[33].

The surface acidity of imogolite was determined by using Hammet indicators adsorbed on the clay and by titrating them in benzene suspension with n-butylamine. The H(Al) form of imogolite was found to be the most acidic while the Na-exchanged form was only slightly less acidic. Imogolite, as with most clays, was found to be more acidic at low relative humidities (ie, less than 8%). In comparison to other clays, imogolite was more acidic than Na-montmorillonite or kaolinite. With regard to the effect of the cation on acidity it was found that H^+ > Al^{3+} > Fe^{2+} > Mg^{2+} > Ca^{2+} > Ba^{2+} > Na^+ > NH_4^+. This order results from the polarizing effect of the cation. The polarizing effect increases with increasing positive charge and with decreasing radius of the ion. Imogolite also shows an increase in acidity upon heating. This is most likely due to the dehydration and dehydroxylation. Imogolite reaches its maximum acidic state around 500°C where dehydroxylation has essentially been completed. At 900°C there is a major loss in acidity due to new mineral formation. The acid

sites of imogolite appear to be generated by the dissociation of the surface hydroxyl groups[34].

LIST OF REFERENCES

1. Pinnavaia, T. J. Science 1983, *220*, 365.

2. Barrer, R. M. "Zeolites and Clay Minerals as Sorbents and Molecular Sieves." Academic Press: New York, 1978.

3. Mortland, M.M. and Berkheiser,V.E. Clays and Clay Miner. 1978, *26*, 319.

4. Traynor, M.F.; Mortland, M.M. and Pinnavaia, T.J. Clays and Clay Miner. 1978, *26*, 319.

5. Barrer, R. M.; McLeod, D. M. Trans. Faraday Soc. 1955, *51*, 1290.

6. Loeppert, R. H., Jr.; Mortland, M. M.; Pinnaivia, T. J. Clays Clay Miner. 1979, *27*, 201.

7. Brindley, G. W.; Semples, R. E. Clay Miner. 1977, *12*, 229.

8. Adams, J. M. Applied Clay Science 1987, *2*, 309.

9. Lahav, N.; Shani, V.; Shabtai, J. Clays Clay Miner. 1978, *26*, 107.

10. Vaughn, D. E. W.; Lussier, R. J. Preprints 5th International Conference on Zeolites; Naples, Italy, June 2-6, 1980.

11. Yamanaka, S.; Brindley, G. W. Clays Clay Miner. 1979, *27*, 119.

12. Johnson, G., Acta Chem Scand. 1960, *14*, 661.

13. Landau, S., Ph.D. Dissertation, Michigan State University, 1984.

14. Theng, B.K.G. "the Chemistry of Clay-Organic Reactions", Wiley, New York, 1974.

15. Van Olphen, H. "An Introduction to Clay Colloid Chemistry", Wiley, New York, 1977.

16. Whitehurst, D.D., J.Chem. Tech., 1980, *44*.

17. Endo, T.; Mortland, M.M. and Pinnavaia, T.J., Clays and Clay Miner. **1980**, *28*, 105.

18. Tilak, D.; Tennkoon, B.; Jones, W.; Thomas, J. M. J. Chem. Soc., Faraday Trans. **1986**, *82*, 3081.

19. Poncelet, G.; Schutz, A. "Chemical Reactions in Constrained Systems" Nato ASI Series, Reidel Publishing Company: Dordrecht, Holland, **1986**.

20. Pines, H., "The Chemistry of Catalytic Hydrocarbon Conversions", Academic Press, New York, 1981.

21. Pinnavaia, T.J.; Johnson, I.D., U.S. Patent 4,621,070, **1986**.

22. Lewis, R.M.; Van Santen, R.A., U.S. Patent 4,637,992, **1987**.

23. Occeli, M.L., in: "Proc. Intern. Clay Conf.",Denver, **1985**, ed. Schultz,L.G.; van Olphen, A.; Mumpton, F.A., Clay Minerals Society, Bloomington, **1987**, 319.

24. Yamanaka, S.;Nishihara, T.; Okumara, F.; Hattori, M., in: Abstracts, 24th Meeting Clay Miner. Soc., **1987**.

25. Yoshinaga, N.; Aomine, S. Soil Plant Nutr. **1962**, *8*, 6.

26. Farmer, V. C.; Fraser, A. R. J. Chem. Soc., Chem. Commun. **1977**, *32*, 462.

27. Farmer, V. C.; Adams, M. J.; Fraser, A. R.; Palmieri, F. Clay Miner. **1983**, *18*, 459.

28. van der Gaast, S. J.; Wada, K.; Wada, S.-I.; Kukuto, Y. Clays Clay Miner. **1985**, *33*, 237.

29. Russel, J.D.; McHardy, W.J. and Fraser, A.R. Clay Minerals, **1969**, *8*, 87-88.

30. Cradwick, P.D.G.; Farmer, V.C. and Russell, J.D. Natural Physical Science, **1972**, *240*, 188.

31. Goodman, B.A. et. al. Phys. Chem. Minerals, **1985**, *12*, 342-346.

32. Farmer, V.C. U.S. Patent 4252779, 1981.

33. Wada, K. "Minerals in Soil Enviroments", Soil Science Society of America, Madison, Wisconsin, **1977**.

34. Henmi, T. and Wada, K. Clay Miner. **1974**, *10*, 231-236.

CHAPTER II

Synthesis and Characterization of a Novel
Family of Pillared Clays

2.1 Introduction

The ability of smectite clays to intercalate a variety of guest molecules between silicate host layers of intrinsically high surface area and acidity makes them especially attractive as sorbents and heterogeneous catalysts. Metal oxide pillared clays[1-10] with thermal stabilities above 500°C have revitalized interest in the use of clay intercalation compounds in the petroleum cracking industry. These materials typically are prepared by the intercalation of a polyoxo cation precursor (eg., $Al_{13}O_4(OH)_{24}(H_2O)_{12}^{7+}$), followed by calcination to produce a pillaring metal oxide aggregates of molecular dimension.

Several workers have recognized the possibility of directly intercalating metal oxide sol particles into clay galleries.[11-15] One potential advantage of direct metal oxide intercalation is the opportunity to form "super gallery" pillared clays[15] in which the gallery height is two or more times as large as the van der Walls thickness of the host layer. An intrinsic problem, however, is obtaining sol particles with a sufficiently uniform shape and size to form intercalates with a regular basal spacing.

The focus of this chapter will be to demonstrate that a novel tubular aluminosilicate imogolite[16-20] can be

regularly intercalated in the galleries of a smectite host clay to form a new type of tubular silicate-layered silicate nanocomposite. Imogolite with an empirical composition $(HO)_3Al_2O_3SiOH$ is a particle with an regular outer diameter of about 23Å, an inner diameter of 8.2Å, and a tube length in the range of 10^2-10^5Å. The structure of imogolite, shown in Figure II.1, can be viewed as being derived from a gibbsite sheet in which orthosilicate groups have condensed on the inner hydroxyl plane at triangular faces above vacant octahedral positions. The condensation reaction causes the SiOAl triangular face to contract, resulting in the curling of the gibbsite sheet and the formation of a tube structure. Twelve edge-shared octahedra are required to close the tube completely. Figure II.2 is a schematic representation of the cross section of a completely closed imogolite tube.

Tubular-silicate layered silicate intercalation compounds, herein abbreviated TSLS complexes, represent a new family of pillared clays insofar as the pillaring agent itself is a microporous sol particle with a pore dimension in the molecular size range. In the present work the objective is to describe the synthesis and properties of the TSLS complex derived from imogolite and montmorillonite. Emphasis is placed on those properties relevant to the potential utilization of TSLS complexes for selective adsorption and catalysis.
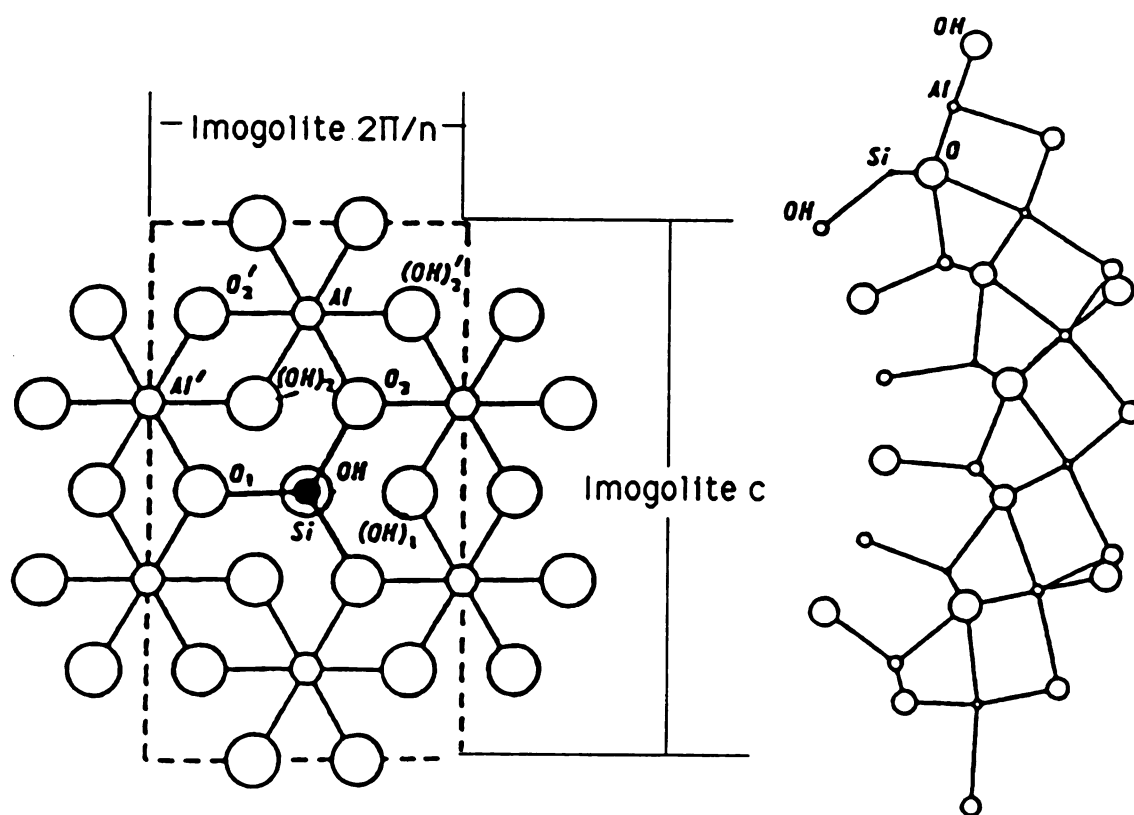
Figure II.1   Idealized structure of imogolite showing con-
densation of an orthosilicate group in a
gibbsite sheet.

○ o SI

● • Al

◯ ◯ O

● ● OH
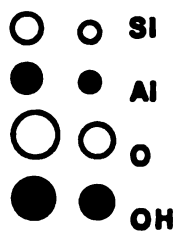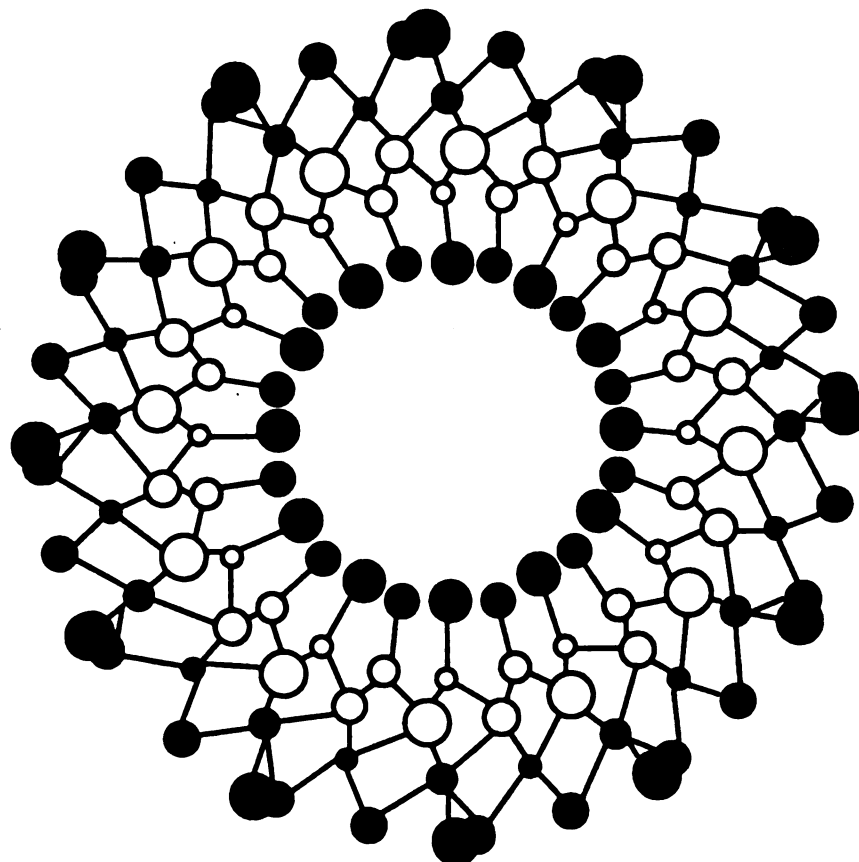
Figure II.2   Schematic representation of the cross section
of an imogolite tube. The outer diameter is
23Å and the inner diameter is 8.5Å.

2.2 Materials

The host clay used in this work was Wyoming Na^+-montmorillonite obtained from the Source Clay Mineral Repository, University of Missouri, Columbia, Missouri. The Na^+-montmorillonite was purified by preparing a 2.5 wt% aqueous suspension and allowing the coarse fraction to sediment over a period of 24 hrs. The suspended fraction was then collected, centrifuged, and treated at 70°C with an acetate-acetic acid buffer at pH 5.0 to remove calcium carbonate. Free non-lattice iron oxides were removed by treating the clay with 1.0M sodium carbonate, followed by subsequent treatment at 80°C with 1.0M sodium thiosulfite in the proportion 1 mL/g clay. Hydrogen peroxide (15%) was used in the proportion 1 mL/g clay in a 1 wt% suspension to remove organic impurities. The clay was then sodium saturated with 1.0M NaCl. The flocculated particles were centrifuged and washed free of chloride ions. The final aqueous suspension was adjusted to a concentration of 1.0 wt%. The unit cell formula of the montmorillonite was $Na_{0.60}[Al_{3.23} Fe_{0.42} Mg_{0.47}] (Si_{7.88} Al_{0.13}) O_{20} (OH)_4$[21].

2.3 Physical Measurements

A Rigaku rotating anode X-ray diffractometer with CuK radiation was used to measure d(001) basal spacings. The samples were prepared for X-ray analysis by air drying 1 mL of a 1 wt% suspension of clay onto a glass slide. The X-ray diffraction patterns were then monitored as a function of

temperature.

BET surface area measurements were taken on a Quantachrome Quantasorb Jr. at liquid nitrogen temperatures with nitrogen as the adsorbate and helium as the carrier gas. The three point BET method was used to determine surface areas. All outgassed samples were heated under vacuum for 24 hrs.

Adsorption isotherms of organic and inorganic molecules with various kinetic diameters were measured on a McBain balance using quartz glass buckets and springs. The probe molecules used for adsorption were water, nitrogen, benzene, 1,2,3,5 tetramethyl benzene, and perfluorotributylamine with kinetic diameters of 2.65, 3.64, 4.3, 5.85, 8.6 and 10.2Å respectively[22]. The liquid adsorbates were kept in a constant temperature bath 5 degrees below room temperature to avoid liquid condensation on the adsorbents at high P/P_o.

Differential thermal analysis, differential scanning calorimetry and thermogravimetric analysis were carried out on a DuPont 9900 thermal analyzer. All samples were run at 10°C per minute under an inert atmosphere of nitrogen.

Infrared spectra were collected on a IBM IR44 FTIR with a resolution of 2 cm^{-1}. All samples were prepared by air drying 1 mL of a 1 wt.% suspension onto a silicon wafer. The samples were then placed in a high temperature cell, evacuated and heated where indicated.

Elemental analysis were performed on a Jarnell-Ash auto-comp ICP emission spectrophotometer. NBS plastic clay

98a served as a standard. The clay samples were prepared by adding 0.05 g of clay sample to 0.3 g of lithium borate (Aldrich Gold Label). The samples were then mixed and fused at 100°C for 12 minutes in graphite crucibles. The resultant glass was dissolved in 50 ml of 6% nitric acid then diluted to 100 ml in distilled water.

Solid state ^{29}Si MAS NMR were carried out on a Varian BRX 400 NMR equipped with Varian computer software and a Doty solid state probe. Talc with a chemical shift of -98.1 ppm served as a reference. Spectra were collected at a Si frequency of 79.459 MHz. The spinning rate was between 5.0 and 8.0 KHz.

The cation exchange capacity of the TSLS complex was determined by exchanging 50 mg of the material with 100 mL of a 1 M solution of ammonium chloride for 24 hours. The clay was washed until the presence of chloride ion could no longer be detected, air dried, and then added to 50 mL of deionized water and stirred. A standardized ammonia electrode was used to determine the concentration of ammonia liberated upon the addition of 5 mL of 10 M sodium hydroxide. The sample was washed, air dried, and weighed, and the cation exchange capacity was determined.

2.4 Imogolite Synthesis

This compound was synthesized by methods analogous to that described by Farmer[23]. Two synthesis procedures were used which differed only in the concentrations of reactants. In the first synthesis a 10-mL portion of Al(sec-BuO)$_3$ (0.040 mol) was allowed to hydrolyze for 4 hr in 250 mL of 0.1 M HClO$_4$ at room temperature. The resulting aluminum solution was then transferred to a 2000-mL round bottom flask to which 650 mL of water and 5 mL of Si(OEt)$_4$ (0.022 moles) was added with stirring. The resulting solution was brought to pH 5.0 by the dropwise addition of about 10 mL of 1.0M NaOH and then immediately brought back to pH 4.0 by the dropwise addition of about 5 mL of 1.0 M acetic acid. The reaction mixture was heated at 98°C for 48 hours until the solution became clear, indicating the formation of imogolite. The second synthesis was identical with the exception that the concentrations of aluminum and silicon were reduced by a factor of two.

The imogolite was then purified by dialysis for a period of 5 days. The dialysis tubing had a molecular weight cut off range of 12,000-14,000. The dialyzing water was changed every 2 hours for the first 10 hours and then every 12 hours for the remaining time. The dialysis was done in order to remove any silica formed during synthesis. The presence of imogolite was verified by the addition of 1.0 M NH$_4$OH to a small volume of the solution and observing the formation of a translucent gel.[17] Also, the air dried

product synthesized at the reduced concentration exhibited a single sharp ^{29}Si MAS NMR resonance at -79 ppm and an infrared band at 348 cm^{-1} characteristic of an Al-O stretch found in imogolite and also in several other clay minerals[17]. The imogolite which was synthesized at the higher concentrations of aluminum and silicon also exhibited an infrared adsorption band at 348 cm^{-1}. However, the ^{29}Si MAS NMR for this product exhibited, in addition to a sharp imogolite resonance near -79 ppm, several broad resonances upfield of the imogolite resonance. The additional resonances were attributed to impurities which formed during synthesis. The latter products, however, was suitable for the formation of a TSLS complex, because the impurities do not bind to montmorillonite and are easily removed by washing.

2.5 TSLS Complex.

The imogolite-montmorillonite intercalation complex was prepared by the dropwise addition of a 0.9 wt.% imogolite suspension into a vigorously stirred 1 wt.% suspension of Na$^+$-montmorillonite. The weight ratio of imogolite:clay used in the reaction was 1.8:1. After having been stirred for 4 hrs at room temperature, the suspension was collected by centrifugation, washed four or more times with water until the presence of imogolite in the washings no longer was indicated by the gel test. The resulting 1 wt.% TSLS complex was then air dried on glass.

2.6 Results

The reaction of dilute aqueous suspensions of synthetic imogolite and Na^+-montmorillonite in 1.8:1.0 (wt/wt) ratio leads to the spontaneous formation of a TSLS complex with a regular intercalated nanocomposite structure. Evidence for regular intercalation is provided by the X-ray diffraction pattern shown in Figure II.3A for an air-dried oriented film sample. At least three rational orders of 001 reflection are observed, corresponding to basal spacings of 38.6Å 0.02Å. This value is in accord with the van der Waals radius of the imogolite tube (25Å), thickness of a clay layer (9.6Å) and a partial hydration shell for the tubes (4.0Å). This agreement between the expected value and the experimentally observed value, along with the relatively high degree of 001 ordering exhibited in the XRD patterns, establishes that the imogolite tubes are indeed intercalated between the clay layers and not just simply adsorbed as a separated phase on the external surface of the clay layers.

Decreasing the imogolite:montmorillonite ratio to 0.9:1.0 leads to incomplete intercalation of the montmorillonite. Figure II.3B shows the X-ray diffraction pattern for a reaction product formed at this weight ratio. The reflections at 12.6, 6.2, and 3.1 Å are attributed to the first three 001 orders of Na^+-montmorillonite that has
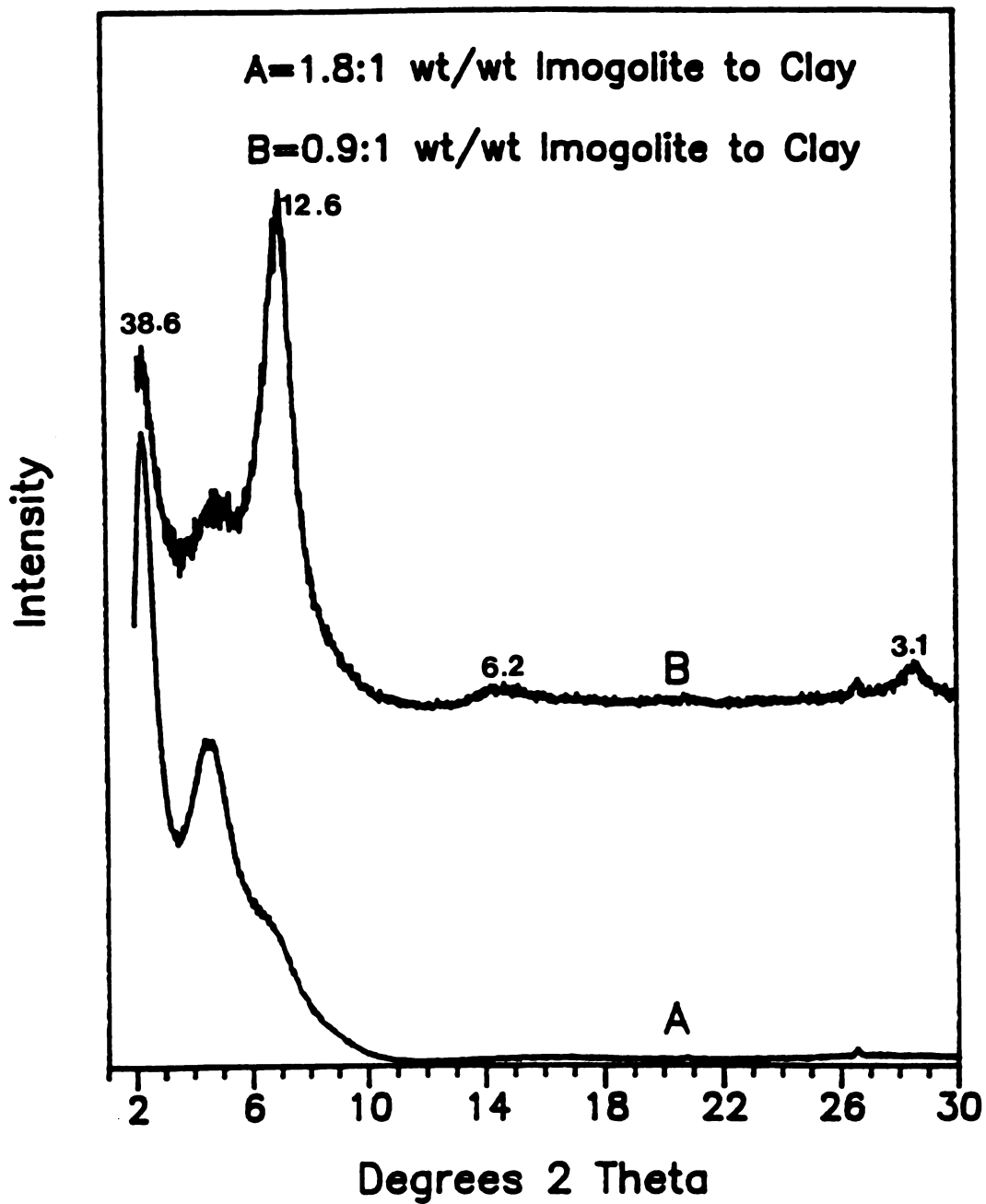
Figure II.3   X-ray diffraction pattern of air dried TSLS
complex using different ratios of imogolite to
montmorillonite.

not been intercalated by imogolite. Spatial considerations suggest there should be sufficient imogolite present to form a complete monolayer of intercalated tubes. However, the presence of unintercalated montmorillonite indicates that a substantial excess of imogolite is required to obtain a completely exchanged TSLS complex.

A sample of imogolite was air dried on the surface of sheet mica and glass to demonstrate that the diffraction pattern for the TSLS complex in Figure II.3A is indeed due to imogolite intercalated between the host clay layers and not just simply stacked on the external surface of the montmorillonite. If the imogolite tubes were bound to the surface of the host clay then the X-ray diffraction pattern obtained should resemble the diffraction patterns for imogolite adsorbed on mica or glass. These results are given in Figure II.4, II.5, and II.6. Figure II.4 is the X-ray diffraction pattern of pure imogolite air dried on a glass slide. It exhibits a very broad peak near 25Å and a second broad peak near 8Å. The second broad diffraction is associated with intertubular bundling caused by the random orientation of the imogolite on the surface. These results are in agreement with those found by Farmer[18]. Figure II.5 is the diffraction pattern of pure sheet mica. This diffraction pattern exhibits several orders of 001 reflections, as expected for such a highly ordered material. These reflections are at 10.0, 5.0, 3.3, and 2.5Å respectively. Figure II.6 gives the diffraction pattern
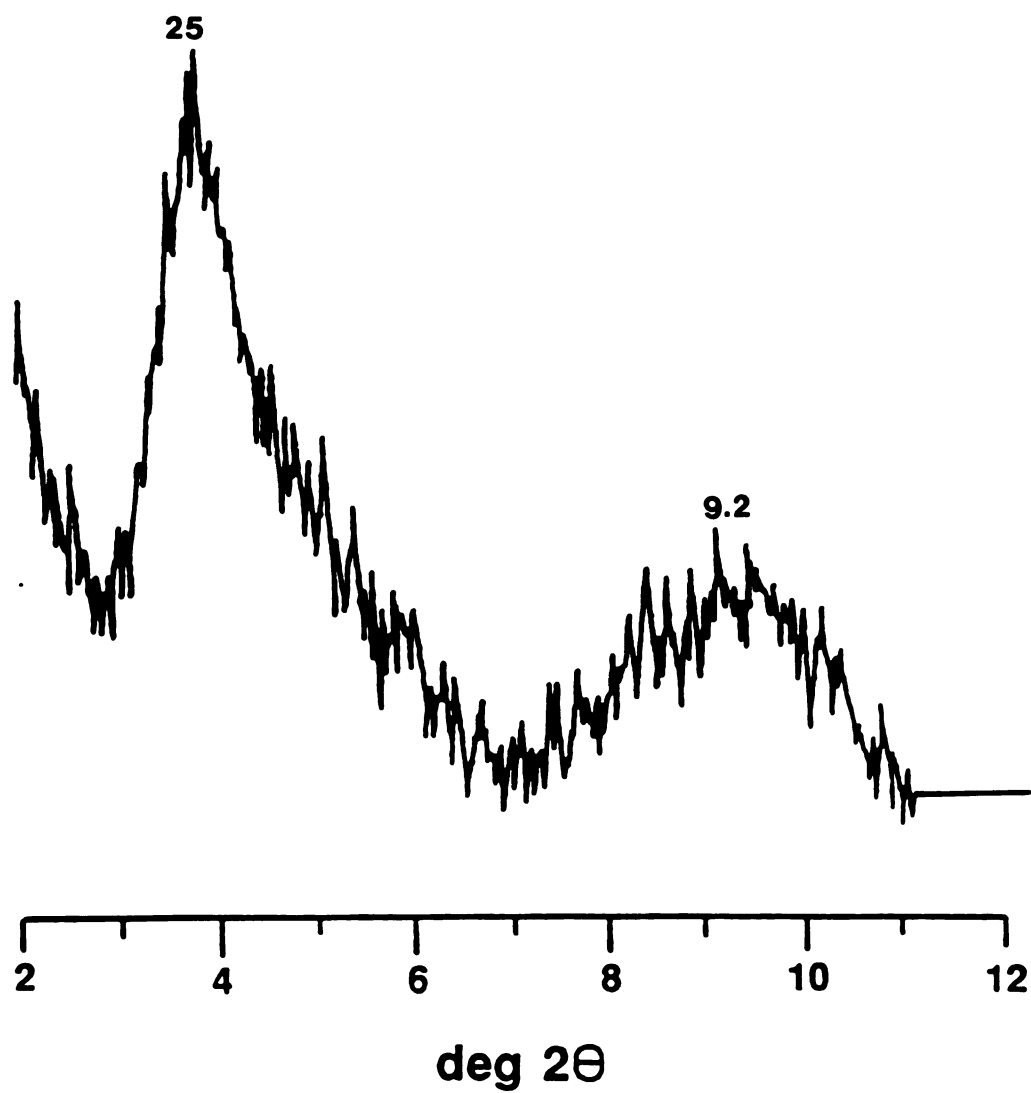
Figure II.4   X-ray diffraction pattern of pure imogolite
               air dried on a glass slide at room
               temperature.
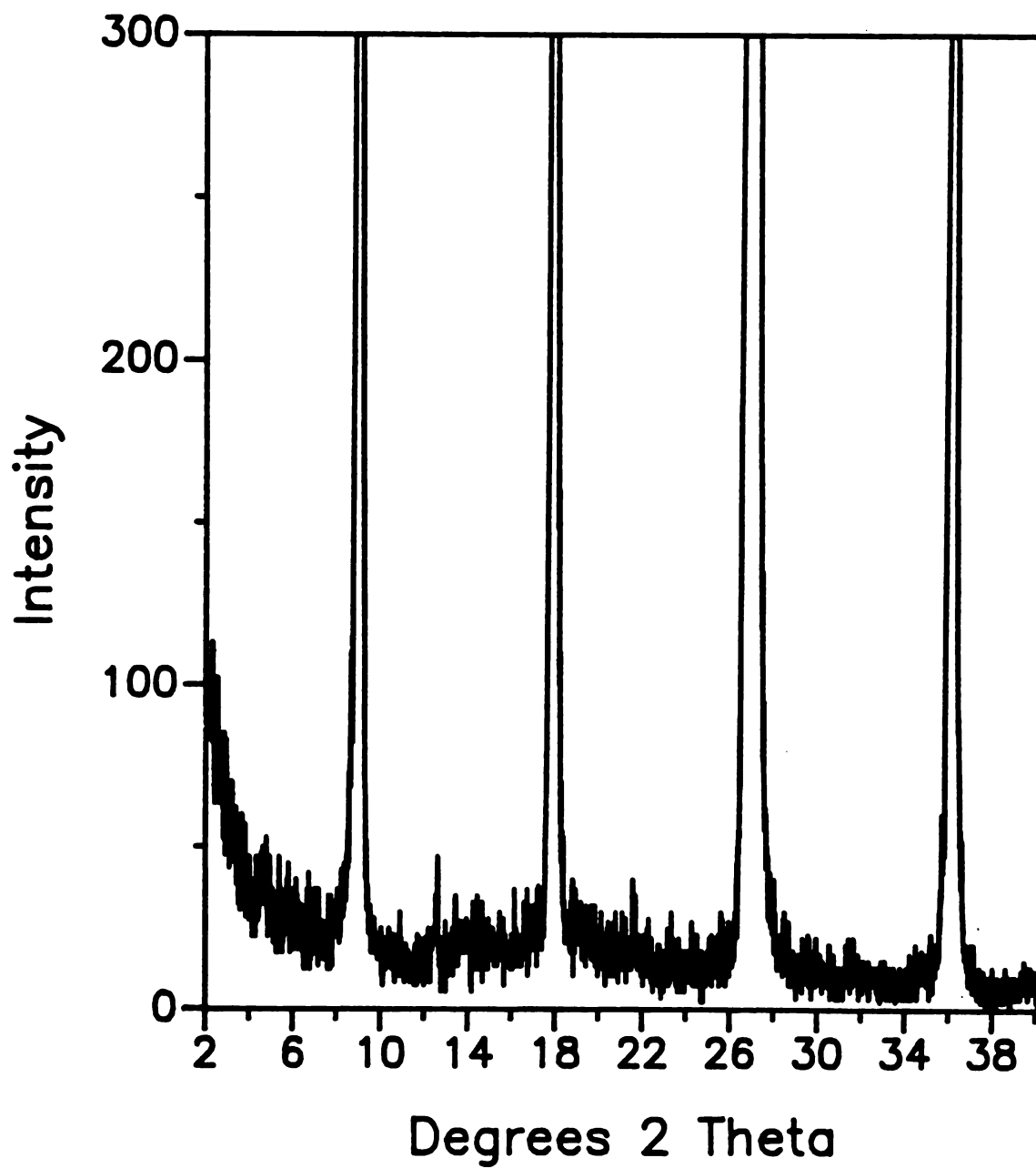
Figure II.5   X-ray diffraction pattern of sheet mica on a
glass slide at room temperature.
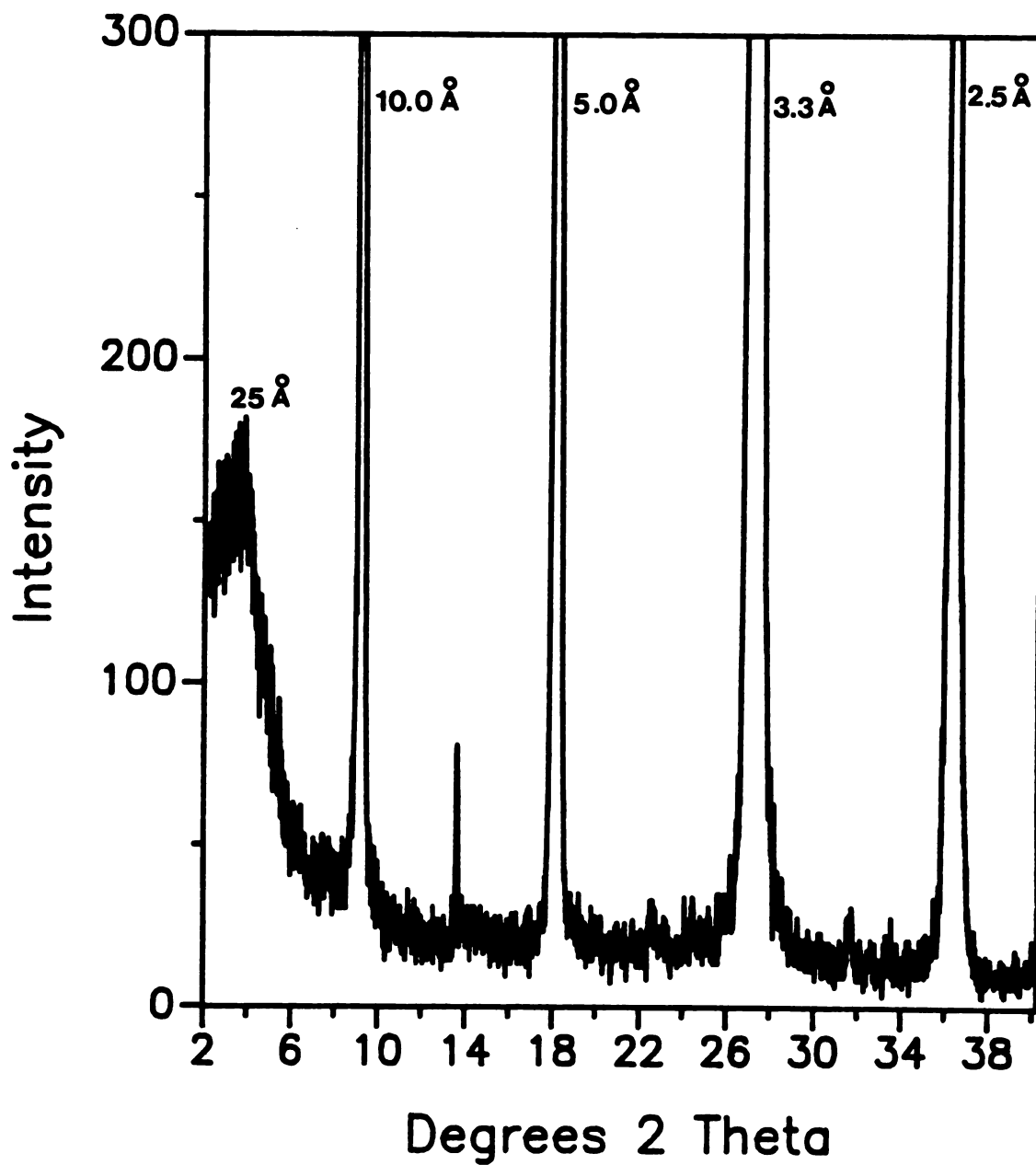
Figure II.6   X-ray diffraction pattern of pure imogolite air
dried on a single piece of mica at room
temperature.

of imogolite air dried on the surface of the sheet mica. As was expected, this x-ray diffraction pattern is essentially the composite of the imogolite X-ray diffraction pattern and the sheet mica X-ray diffraction pattern. This provides substantial evidence for the fact that the imogolite tubes are indeed intercalated between the layers of the montmorillonite and not just adsorbed onto the surface. If the imogolite tubes were adsorbed on the surface of the montmorillonite and not intercalated then one would expect to see similar results to those obtained for the imogolite air dried on the sheet mica. It is quite evident that there is a significant difference in the X-ray diffraction patterns of these two materials.

^{29}Si MAS NMR was used to determine the affect of intercalation on the structure of the imogolite tubes. Pure Na^+-montmorillonite exhibits a resonance peak at -93.5 ppm typical of a Q^3 site in which there are three SiOSi linkages to each silicon. In addition, a weak resonance is observed at -109 ppm due to a silica impurity[24]. Pure imogolite synthesized at the lower concentration of silicon (0.17 M) and aluminum exhibits a single resonance at -79.3 ppm, as shown in Figure II.7, indicative of a Q^0 site in which there are no SiOSi linkages[25]. As shown in Figure 8 the ^{29}Si MAS NMR of the TSLS complex contains the same three resonances at -79.3 ppm, -93.5 ppm and -108.8 ppm found in the parent end members. Thus, there is no structural rearrangement of either the imogolite or of the
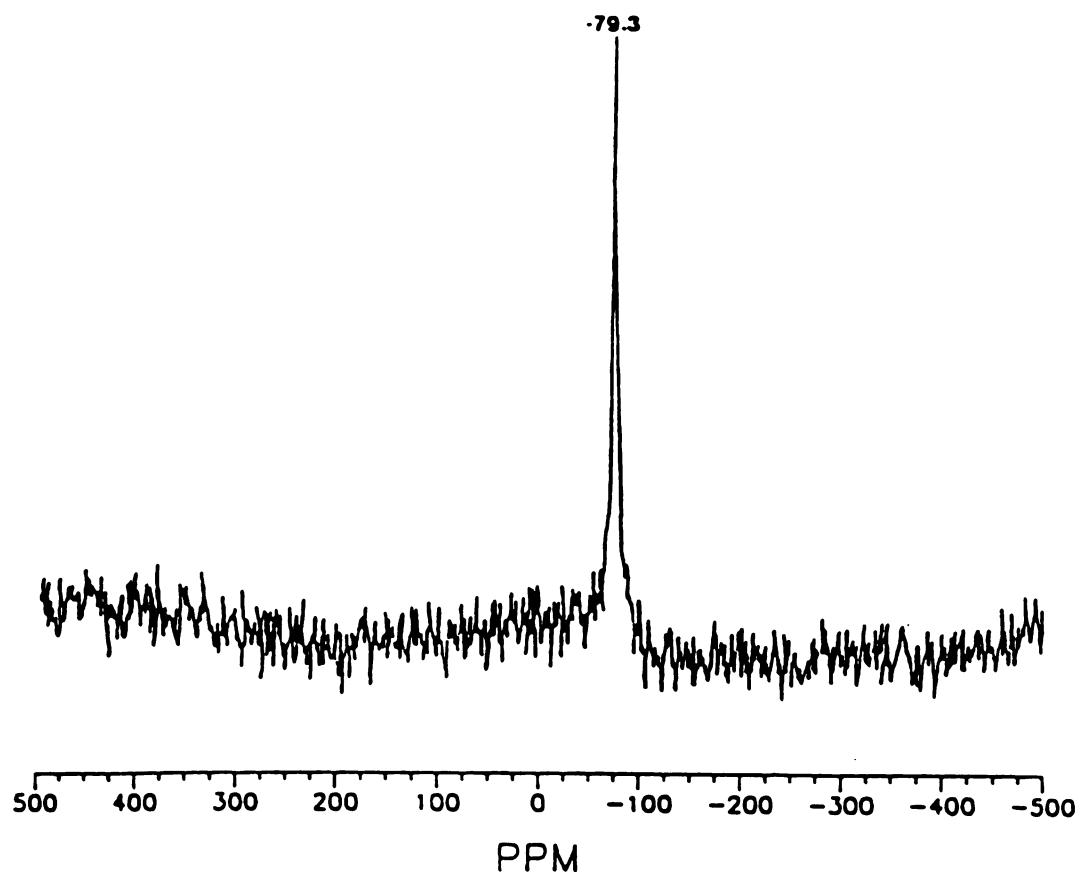
Figure II.7 ^{29}Si MAS NMR of pure imogolite prepared from
dialyzed imogolite. Spectra were collected at
300 MHz using a 4 microsecond pulse width and a
recovery delay time of 2.0 seconds. The reson-
ance at -79.3 ppm is assigned to the resonance
of a Q^0 silicon in imogolite. Samples were
pre-pared by air drying, grinding and packing
them in a saphire rotar.
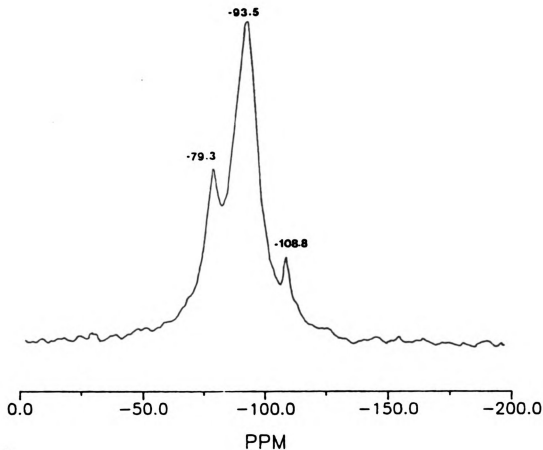
Figure II.8 ^{29}Si MAS NMR of the TSLS complex prepared from
              dialyzed imogolite and Na$^+$-montmorillonite.
              Spectra were collected at 300 MHz using a 4
              microsecond pulse width and a recovery delay
              time of 2.0 seconds. The resonances at −79.3,
              −95.5 and −108.8 ppm are assigned to the
              resonances of imogolite, montmorillonite and
              a silica impurity. Samples were prepared by
              air drying, grinding and packing them in a
              saphire rotor.

montmorillonite upon formation of the TSLS complex.

The ^{29}Si MAS NMR of the TSLS complex synthesized using the imogolite prepared at higher concentrations(0.34 M) shows some interesting characteristics. In the spectrum of the "pure imogolite", the ratio of silicon attributed to imogolite to the silicon of the non imogolite is 1:2.75. However, there is a significant change in the ratio of imogolite silicon to non imogolite silicon after intercalation into the host montmorillonite. The ratio of imogolite silicon to non-imogolite silicon after intercalation is 3.2:1. This significant change in Si ratio indicates that there are two or more different phases of material being made during the imogolite synthesis when using higher concentrations of silicon and aluminum. It is also evident that the non-imogolite phases can be washed out by centrifugation and that the remaining intercalated material is primarily imogolite. The remaining results and discussion of this chapter will deal with the imogolite prepared at the lower concentrations of silicon and aluminum.

The X-ray and ^{29}Si MAS NMR data are consistent with a TSLS structure in which a monolayer of imogolite tubes is intercalated in the galleries of the montmorillonite host. Since the ^{29}Si MAS NMR lines have relative intensities of 0.335:1.0 imogolite : montmorillonite, the corresponding composition of the TSLS complex by weight is 0.36:1.0. On the basis of the van der Waals diameter of imogolite (23Å)

and the unit cell size of montmorillonite (48 $Å^2$) the expected composition for complete filling of the clay galleries by tubes is 0.850:1.0 (wt/wt) imogolite:montmorillonite. Thus, approximately 46% of the interlayer space of the TSLS complex is occupied by imogolite.

If imogolite is electronically neutral, we would expect a CEC of approximately 80 meq/100g for the TSLS complex. It may be that imogolite carries a net positive charge since the TSLS complex was formed below the isoelectric point of the imogolite. A substantial portion of the cation exchange capacity (CEC) of montmorillonite is retained upon formation of the TSLS complex. The CEC, as determined by displacement of Na^+ by NH_4^+, is 45.5 meq/100g of TSLS complex. Since the CEC of the parent montmorillonite is 79 meq/100g, the value observed for the TSLS complex is in reasonable agreement with the overall 0.36 : 1.0(wt/wt) imogolite:montmorillonite composition since the exact charge on the imogolite tubes is not known.

The next area of interest was the thermal properties of the TSLS complex. Figure II.9 provides the differential thermal analysis curves for pure synthetic imogolite and the TSLS complex. Pristine synthetic imogolite exhibits a low temperature dehydration endotherm starting at 30°C, an exotherm between 350°-450°C that is tentatively assigned to dehydroxylation and SiOSi bond formation, and a high
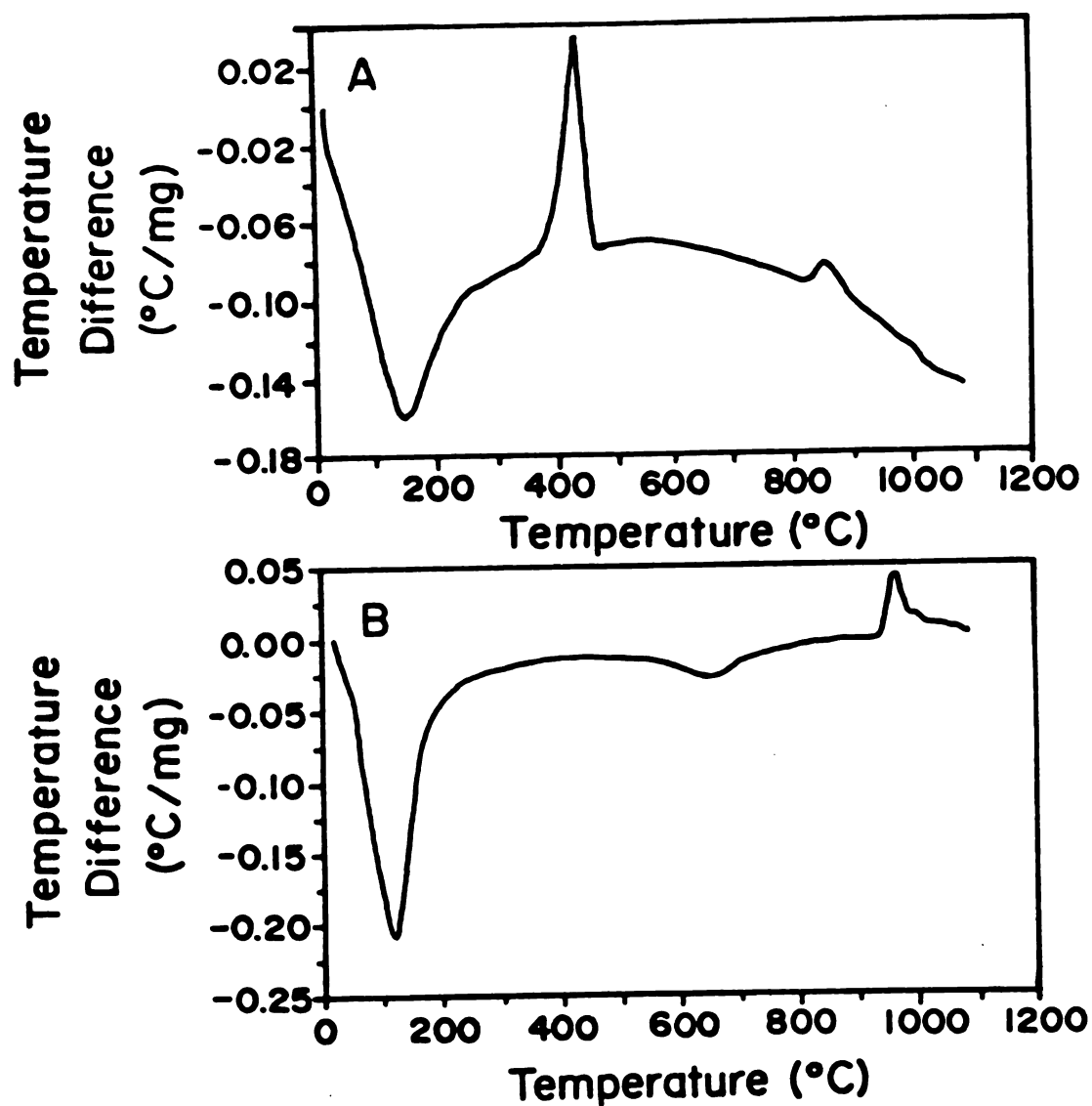
Figure II.9   Differential thermal analysis curves for (A) imogolite and (B) imogolite montmorillonite TSLS complex.

temperature recrystallization exotherm (approx. 800°C). The TSLS complex exhibits, in addition to a high temperature recrystallization exotherm, two endotherms starting at 30°C and 550°C that are attributable to dehydration of the complex and dehydroxylation of montmorillonite respectively[26]. However, the 350°C exotherm characteristic of imogolite is absent from the DTA of the complex, indicating that the thermal properties of imogolite are altered upon intercalation.

To further investigate the origin of the 350°-400°C exotherm for pristine imogolite, we obtained the temperature dependent FTIR spectra shown in Figure II.10. The band at 995cm^{-1} is characteristic of the orthosilicate Si-OH stretch of imogolite[26]. As the temperature is increased above 200°C, the intensity of the band diminishes, and a new silicon oxygen stretching band appears at 1090 cm^{-1}, which we attribute to Si-O-Si bond formation in agreement with previous assignments for natural imogolite[25]. The siloxane bonds most likely arise due to tube collapse and trans-annular condensation of SiOH groups. The appearance of the new siloxane band in the FTIR is correlated with the 350-450°C endotherm in the DTA curve. Apparently, tube collapse is inhibited in the TSLS complex, because the 350°C endotherm is not observed.

Further evidence for the stabilization of the imogolite tube structure in the TSLS complex is provided by N_2 BET surface area measurements. For outgassing temperatures in
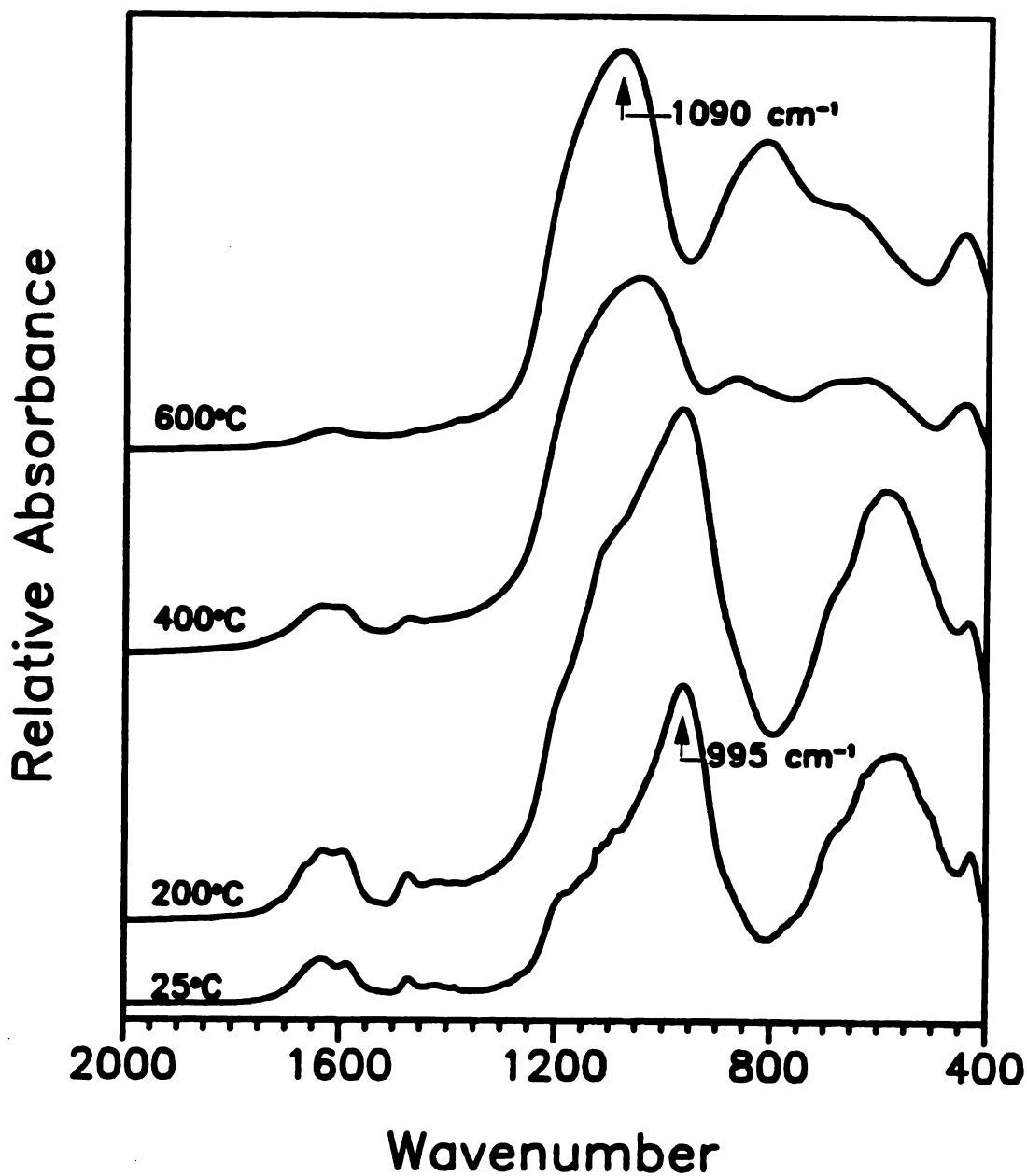
Figure II.10   Temperature dependent FTIR spectra of imogo-
                lite. Samples were prepared by heating to
                the desired temperatures and then pressing
                them into KBr pellets.

the range 125-435°C, the N_2 BET surface area of the complex decreases only slightly from 274 m^2/g to 230 m^2/g. In contrast, the surface area of pure imogolite decreases dramatically from 260 m^2/g to less than 5 m^2/g upon increasing the outgassing temperature from 200°C to 300°C.

As shown by the plot of surface area versus temperature in Figure II.11, the TSLS complex does eventually undergo a dramatic loss in surface area when heated to 500°C. Included in Figure II.11, is the temperature dependence of the d_{001} spacing for the TSLS complex. Interestingly, the loss in surface area is not accompanied by a significant decrease in basal spacing. In fact, as shown by the diffractograms in Figures II.12 and II.13 the complex remains relatively well ordered along the 001 direction even up to 625°C. Thus the clay remains intercalated at elevated temperatures, but, structural rearrangement apparently occurs above 400°C which leads to substantial decrease surface area.

Nitrogen (kinetic diameter = 3.6Å) adsorption and desorption isotherms were obtained for the imogolite-montmorillonite complex at -196°C. The results are given in Figure II.14. The shape of the adsorption isotherm below a partial pressure of 0.5 was very similar to the classical type I isotherm for a microporous material with pore diameters of less than 20Å according to Brunauer et al.[27]. Above a partial pressure of approximately 0.50, tailing of the adsorption isotherm was observed due to mesoporosity in
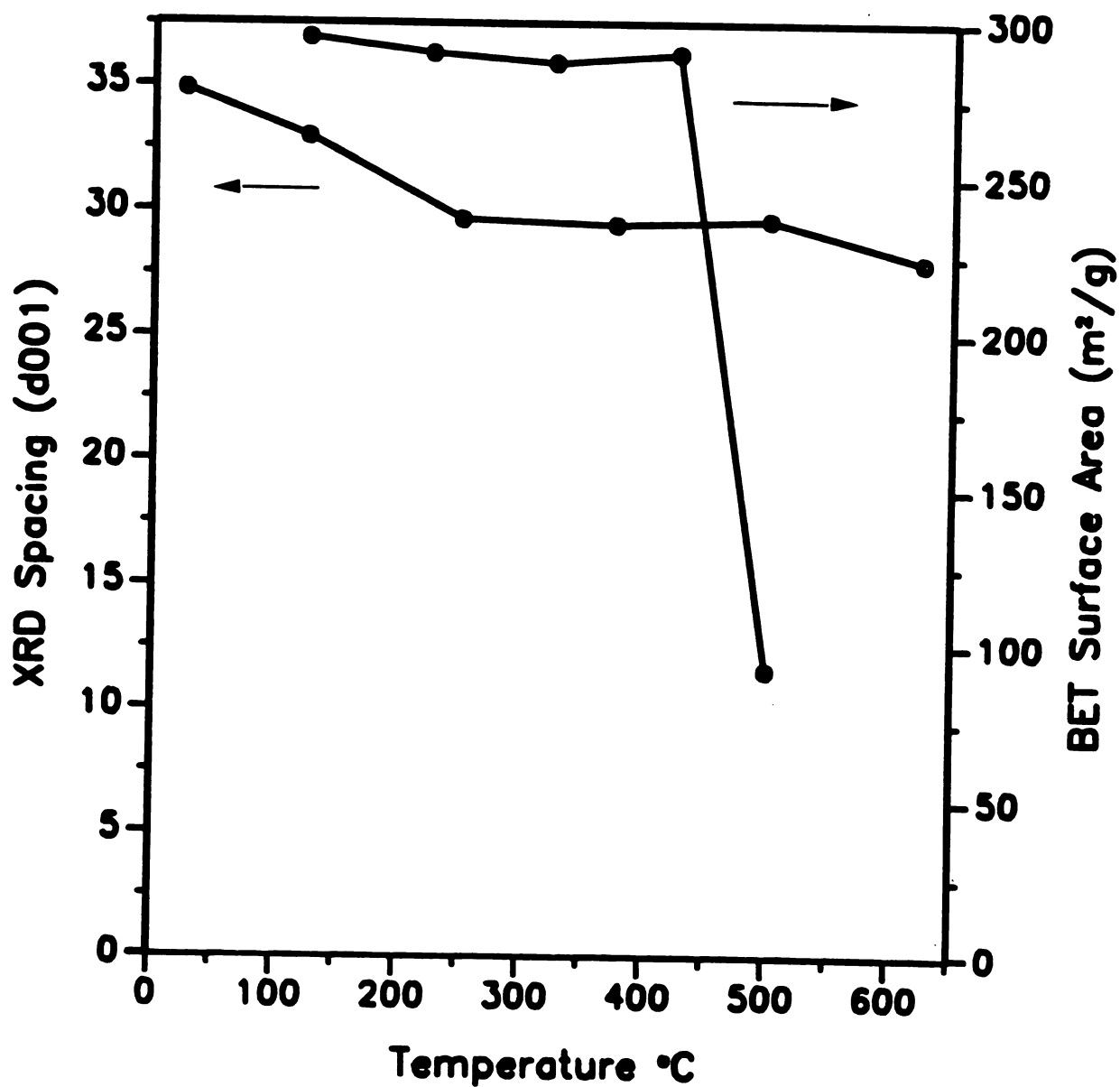
Figure II.11   Plot of surface area and d(001) spacings of
the TSLS complex as a function of temperature.
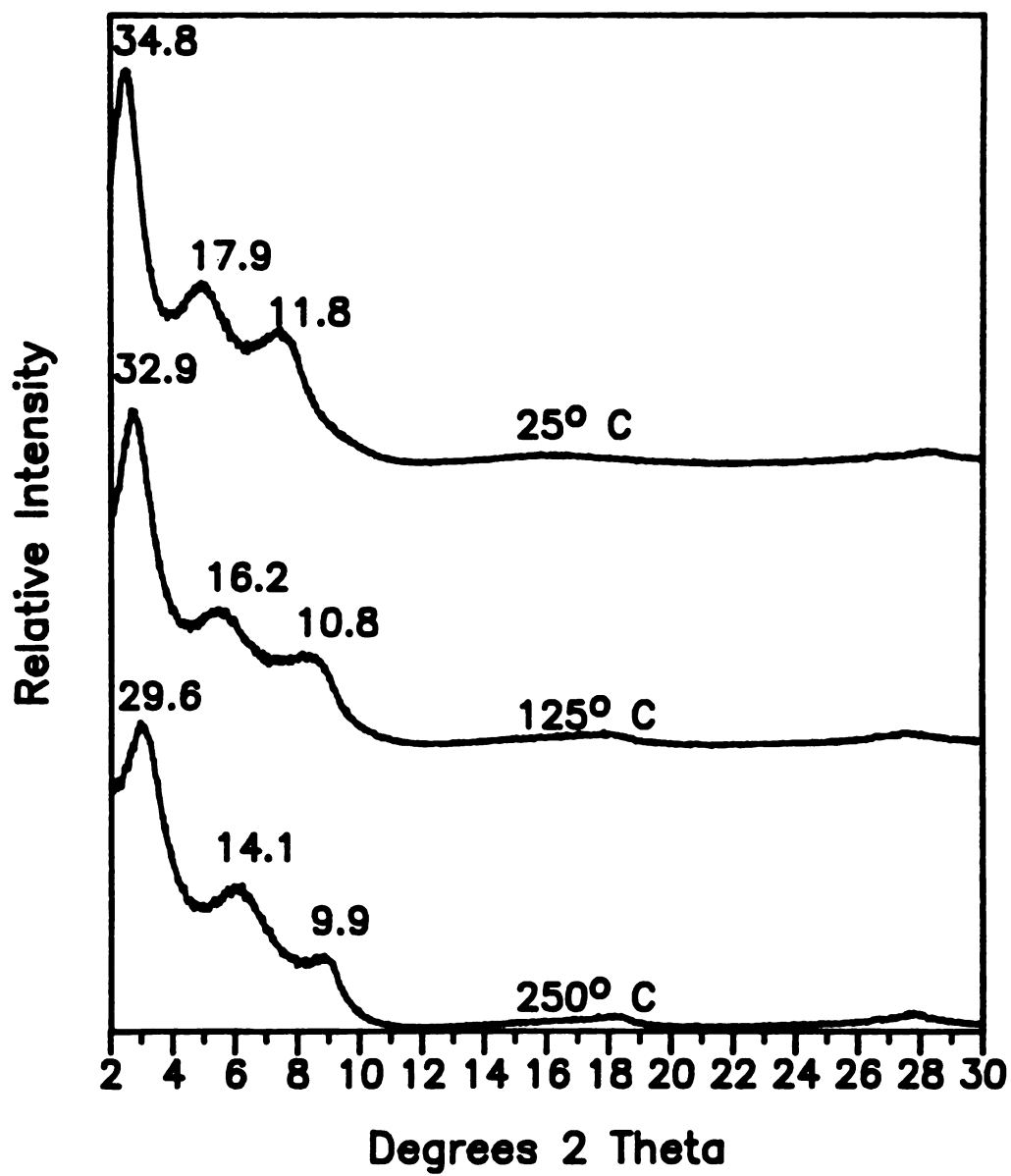
Figure II.12   Temperature dependent X-ray diffraction
               patterns of the TSLS complex.
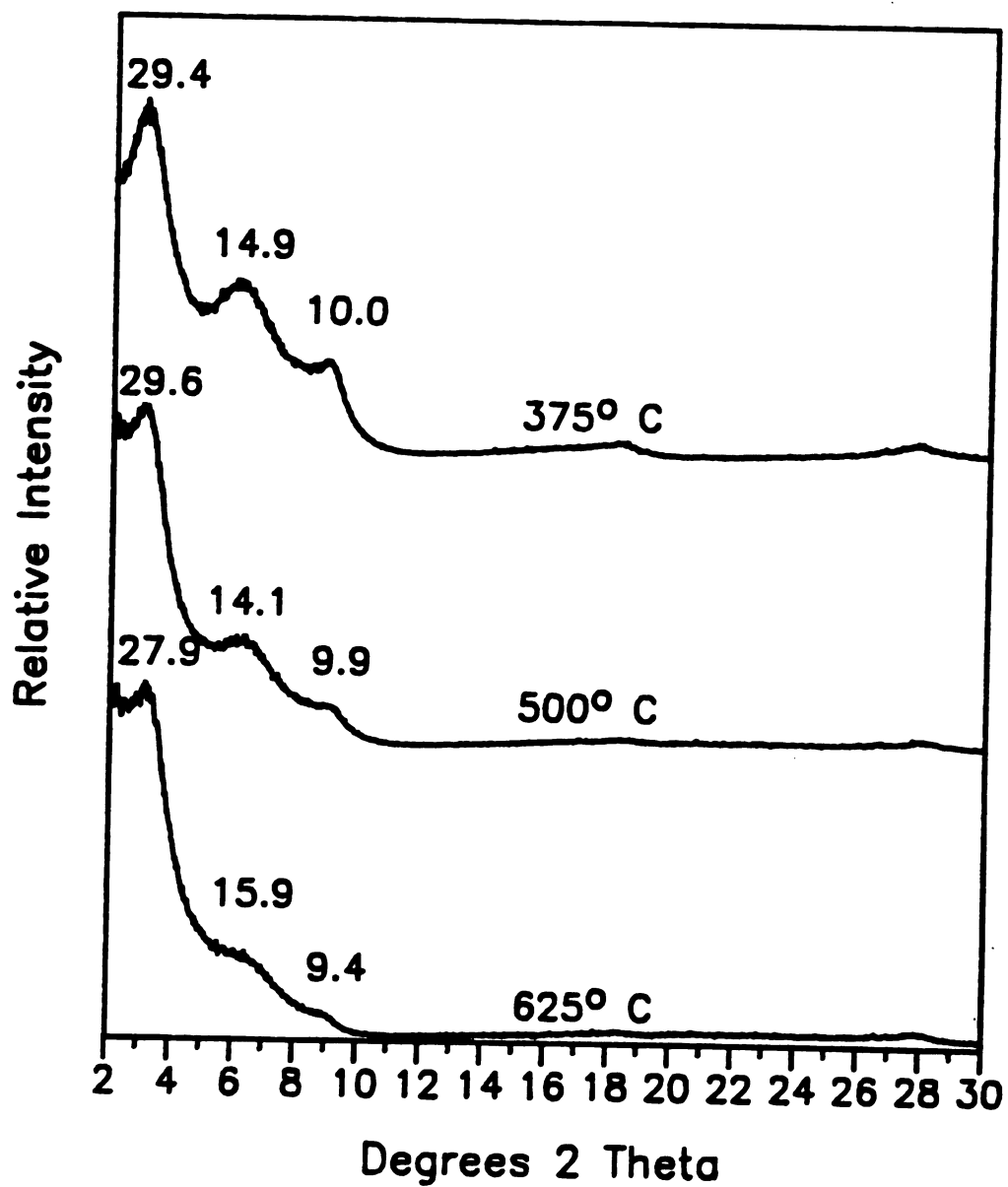
Figure II.13   Temperature dependent X-ray diffraction
                patterns of the TSLS complex.
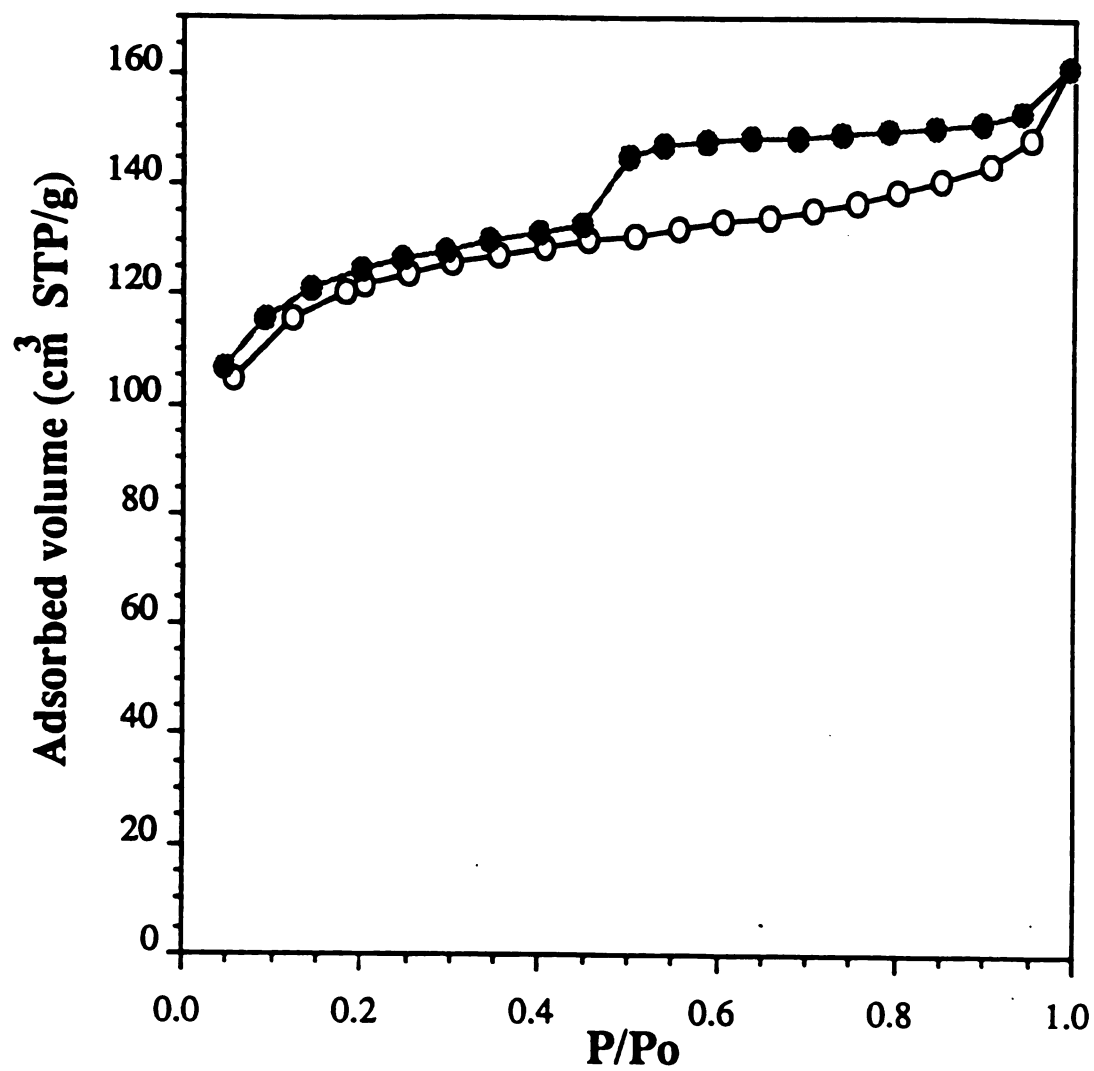
Figure II.14   Nitrogen adsorption/desorption isotherm on
the TSLS complex at 77K.

the range of 20-500Å. The presence of some mesopores was confirmed by the hysteresis loop observed upon desorption.

The nitrogen adsorption data over the partial pressure range $0 < P/P_o < 0.15$ were fitted to the BET equation:[28]

$$\frac{P/Po}{V(1-P/Po)} = \frac{1}{V_mC} + \frac{(C-1)(P/Po)}{V_mC}$$

An equivalent surface area of 460 m^2/g was determined from the monolayer volume, V_m. The value obtained for the dimensionless energetic constant, $C=260$, is characteristic of a microporous material[29]. Although the BET surface area may not be a physically precise quantity due to the fact that the nitrogen molecule does not exhibit the same cross sectional area in a microporous environment as on a flat surface,[29] the BET value is useful for comparisons of relative porosities among a related class of adsorbents. For instance, smectite clays pillared by metal oxide aggregates typically exhibit BET surface areas in the range of 150-400 m^2/g. Thus, the TSLS complex is among the more porous intercalated nanocomposites derived from smectite clays.

The total micro pore volume (V_o) of the TSLS complex was assessed by applying the Dubinin-Radushkevich equation[30] to the nitrogen adsorption data:

$$Log\ V = Log\ V_o + D[log(p/p_o)]^2$$

As shown by the dashed line in Figure II.15, the equation provided a good fit of the data over the low and
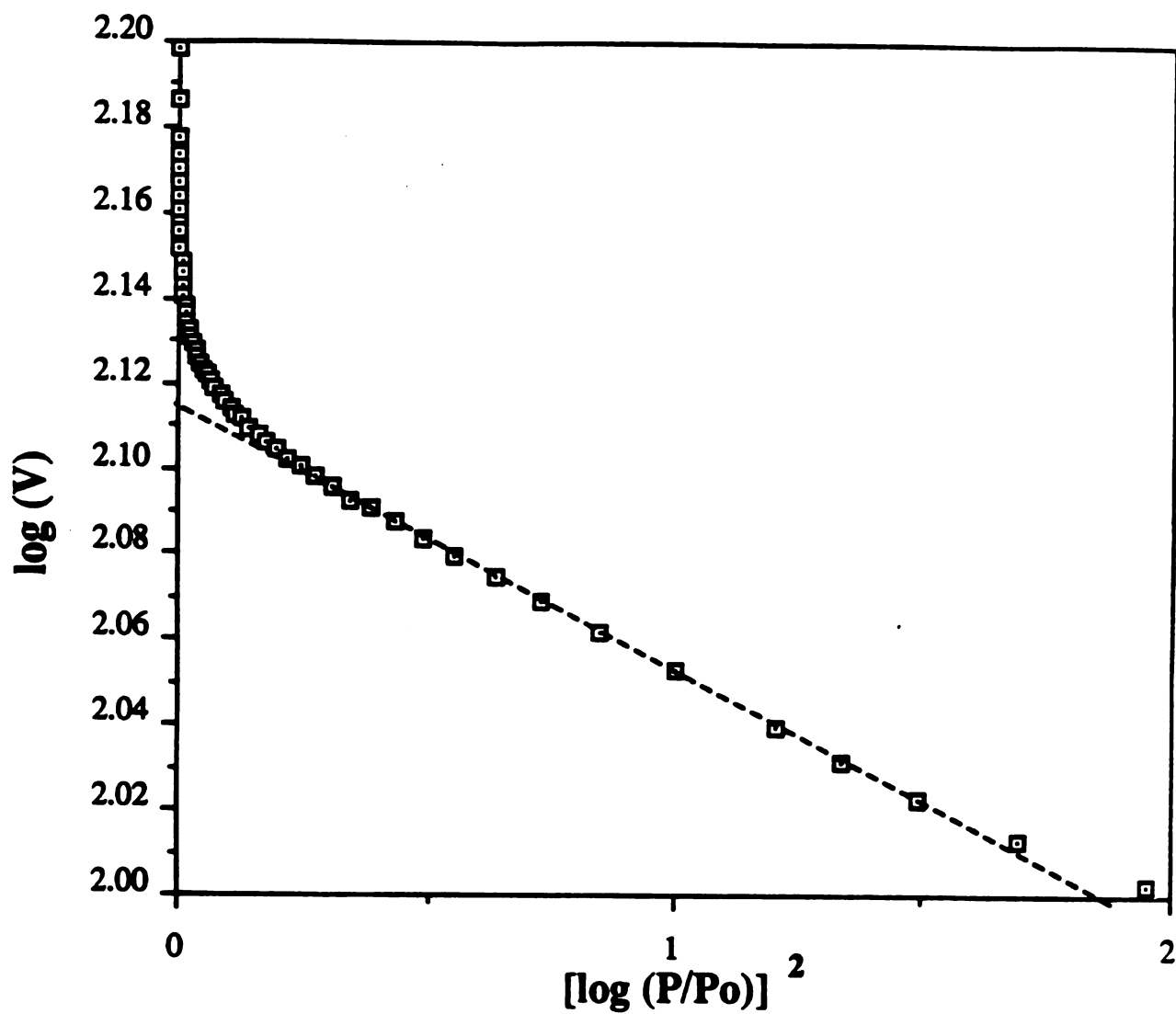
Figure II.15   Dubinin-Radusikevich plot of the nitrogen
adsorption data on the TSLS complex.

intermediate pressure ranges. The intercept of the best straight line fit gave a liquid pore volume V_o = 0.20 cm^3/g.

A t-plot[31] of the nitrogen adsorption data, shown in Figure II.16, exhibited three distinct regions. In the first region, the data were fitted to a straight line passing through the origin. The slope of this line yielded an equivalent surface area of 480 m^2/g, comparable to the value of 460 m^2/g obtained from the BET treatment of the data. Another domain of data points were fitted to a second straight line with an intercept (67 cm^3 STP g^{-1}) corresponding to a microporous liquid volume of 0.10 cm^3/g. A third domain of points yielded an overall liquid volume of 0.16 cm^3/g. The total micropore volume 0.10 + 0.16 = 0.26 cm^3/g is slightly higher than the results obtained from the Dubinin Radusikevich plot (0.20 cm^3/g). This bimodal microporous behavior is consistent with the two types of micropores expected for an intercalated TSLS complex. As illustrated in Figure II.17, there are two types of environments available for nitrogen adsorption, namely, the type A intratubular pores and the type B intertubular pores. It is likely then that this bimodal distribution arises from these two type of environments.

The nitrogen desorption isotherm was treated according to the model developed by Delon and Dellyes for a parallel plate pores in phyllosilicates[32]. The mesopore liquid volume obtained using this treatment was relatively small, 0.03 cm^3/g. Thus, the pore volumes derived from the t-plot
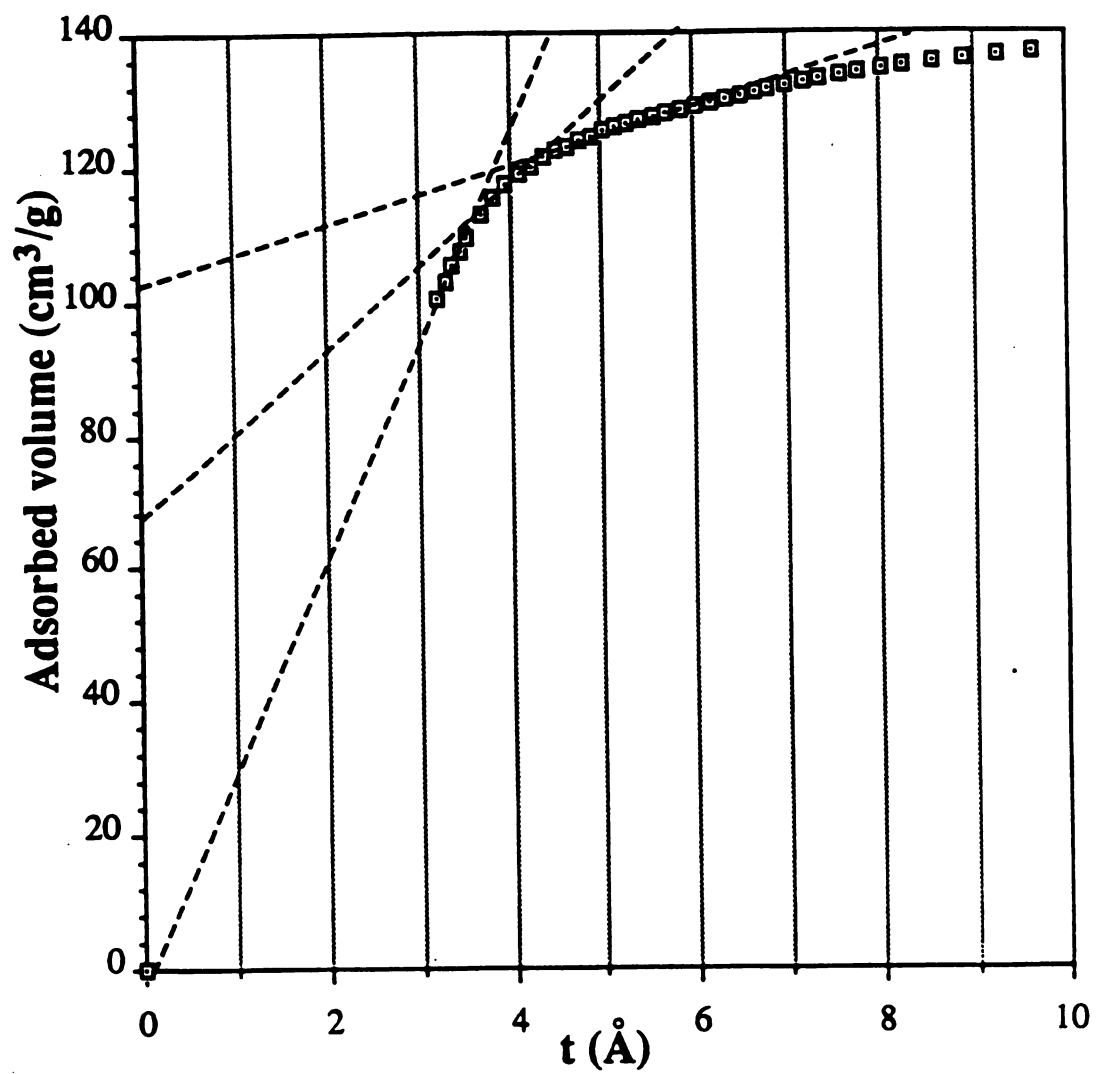
Figure II.16 t-Plot for the nitrogen adsorption data on the TSLS complex.
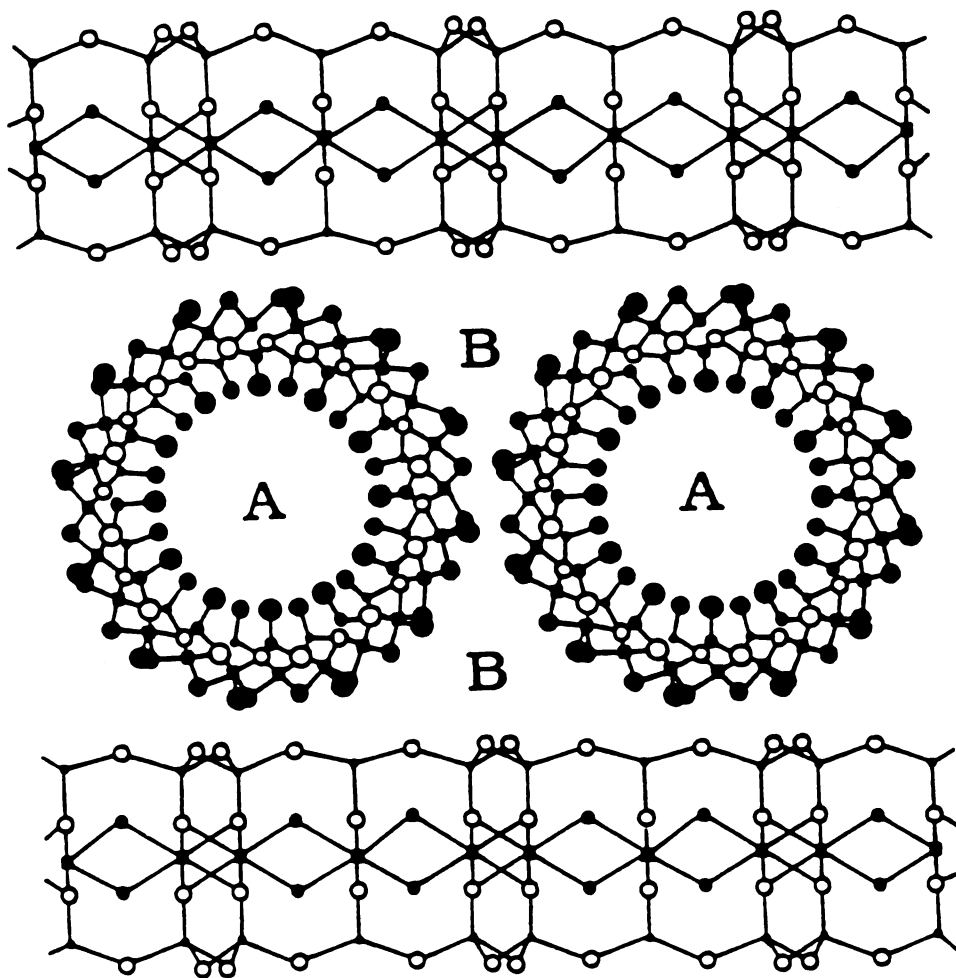
Figure II.17   Schematic illustration of the TSLS structure
formed by intercalation of Imogolite tubes in
the interlayers of Na$^+$-montmorillonite.
A and B denote the two possible types of
micropres.

analysis (0.16 cm^3/g) and the nitrogen desorption branch (0.03 cm^3/g) sum to a value of (0.19 cm^3/g) in good agreement with the pore volume obtained from the Dubinin-Radusikevich equation (0.20 cm^3/g).

In order to examine the adsorption of an organic adsorbate by the TSLS complex, the adsorption isotherm for m-xylene (kinetic diameter, 5.6Å) was obtained at 25°C. As shown in Figure II.18, the shape of the isotherm was again type I, as expected for a microporous adsorbent. The Dubinin-Radusikevich equation provided a reasonable fit of the data over the low and medium partial pressure ranges, as illustrated in Figure II.19. The microporous liquid volume obtained by this treatment was 0.11 cm^3/g. This value was significantly lower than the microporous volume obtained by nitrogen adsorption (0.20 cm^3/g). Thus Gurvitsch's rule[33] which states that the microporous volume should be independent of the adsorbate size does not hold for the TSLS complex. This result suggested that the planar m-xylene molecule, for which kinetic diameter is approximately two thirds the internal 10Å pore diameter of the intercalated imogolite, was geometrically incapable of filling completely the available pore volume. An analogous geometrical effect was believed to be important in determining the adsorbate-dependent filling of the pristine imogolite tubes[34]. Thus, it may be concluded that a substantial portion of the microporous volume of the TSLS complex arises due to
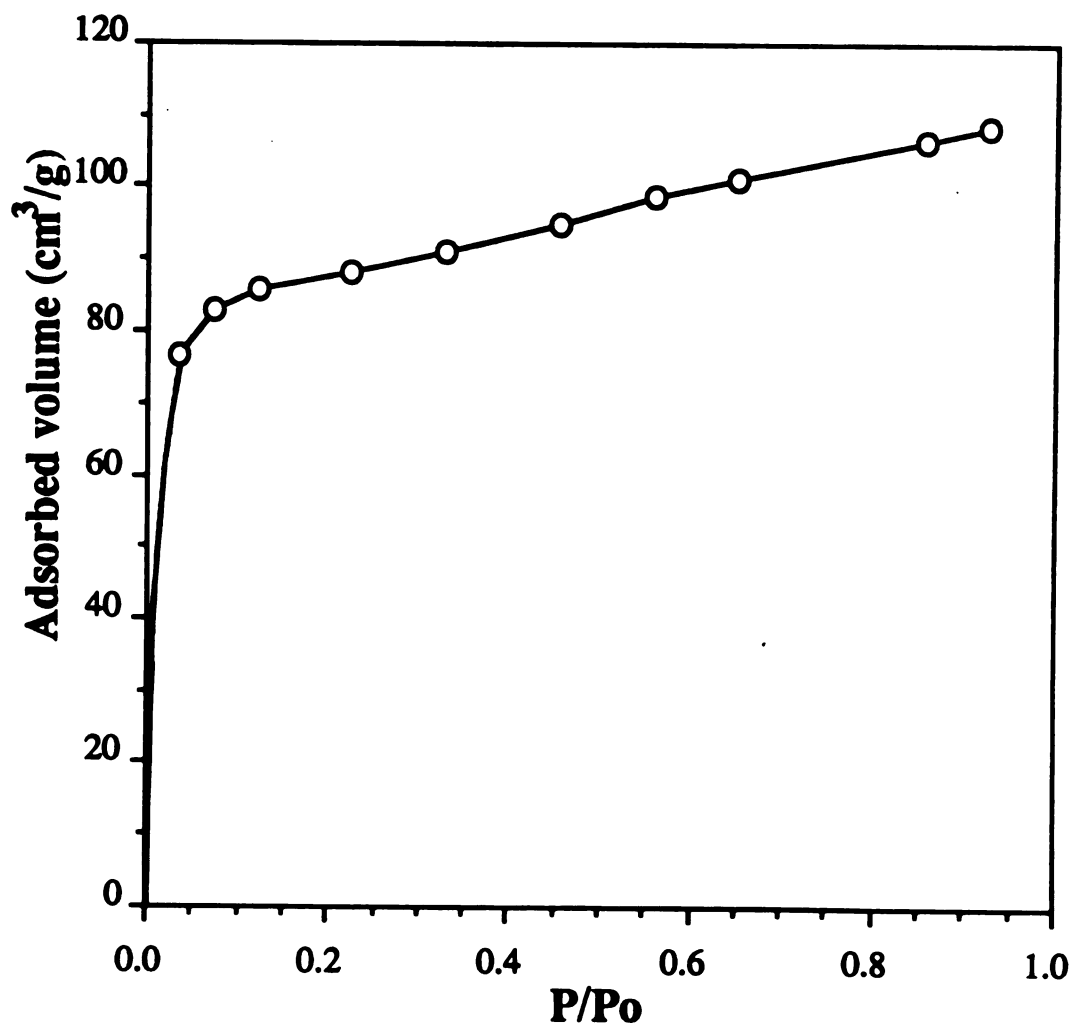
Figure II.18   m-Xylene adsorption isotherm at 298K on the
                TSLS complex.
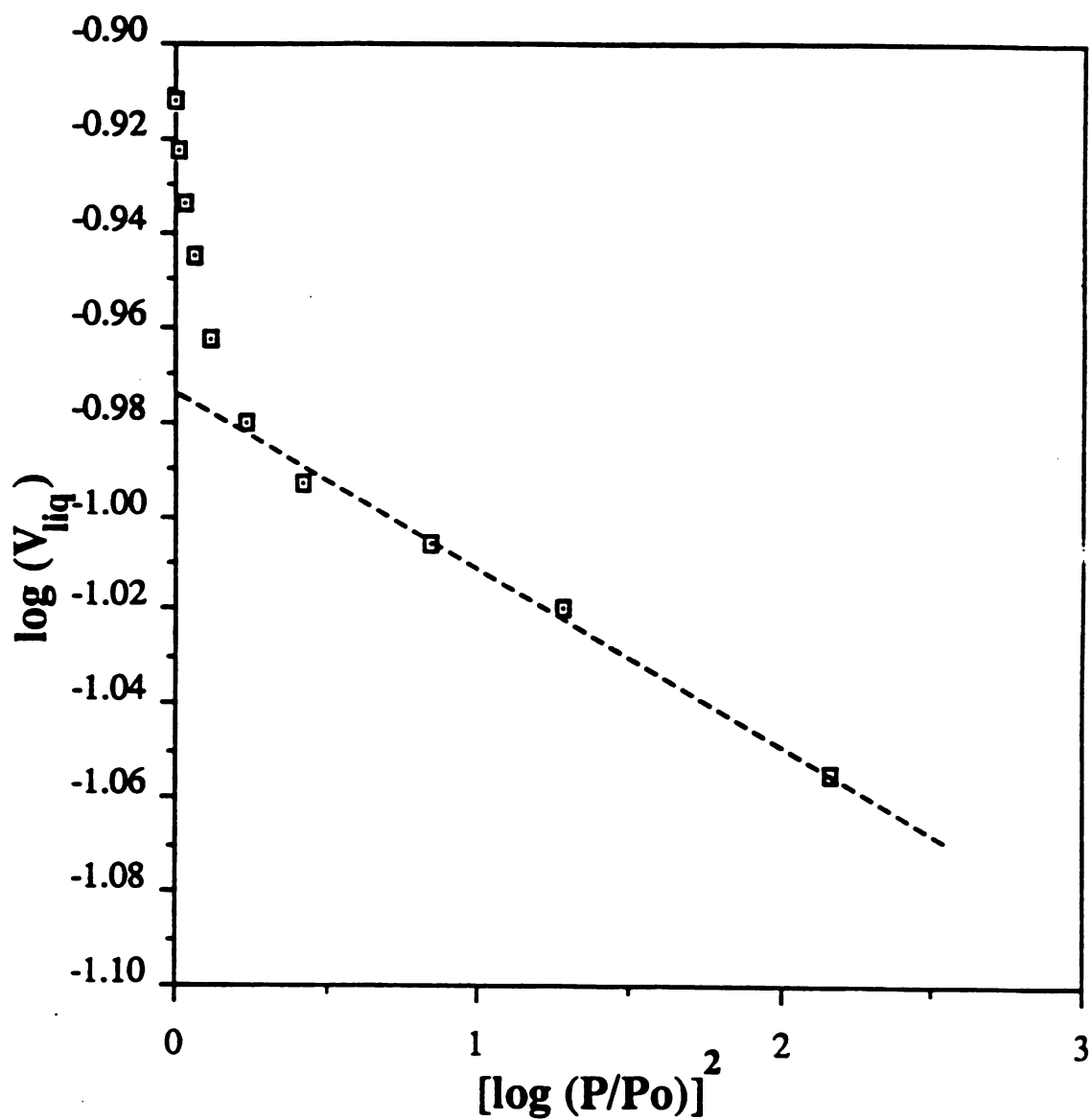
Figure II.19   Dubinin-Radusikevich plot of m-xylene
                adsorption data.

adsorption on the internal surfaces of the intercalated imogolite tubes.

In addition, adsorption isotherms were taken for molecules with various kinetic diameters to determine the molecular sieving properties of the TSLS complex. The kinetic diameters of the probe molecules used ranged from 2.8Å (H_2O) to 10.2Å (perfluorotributylamine). Figure II.20 illustrates the total adsorption capacity of the different adsorbates at a relative pressure (P/P_o) of 0.95. The TSLS complex shows the ability to adsorb a variety of molecules including water, nitrogen, and benzene whose kinetic diameters are less than the internal opening of the imogolite tubes (8.2Å). If the adsorbate used has a kinetic diameter larger than the free space of the imogolite tube then little or no adsorption occurs. This is illustrated by the limited adsorption of perfluorotributylamine. This indicates that the majority of the adsorption capacity of the TSLS complex is intratubular.

2.7 Discussion

The chemical composition of imogolite, when written in the order of outer to inner atomic planes (cf., Figure II.1), is $(HO)_3Al_2O_3Si(OH)$. This novel material occurs in nature as an alteration product in volcanic soils[35], but it also can be prepared by the acid hydrolysis of silicon and aluminum alkoxides[23]. The synthetic analogue used in the present studies has an isoelectric point at slightly basic
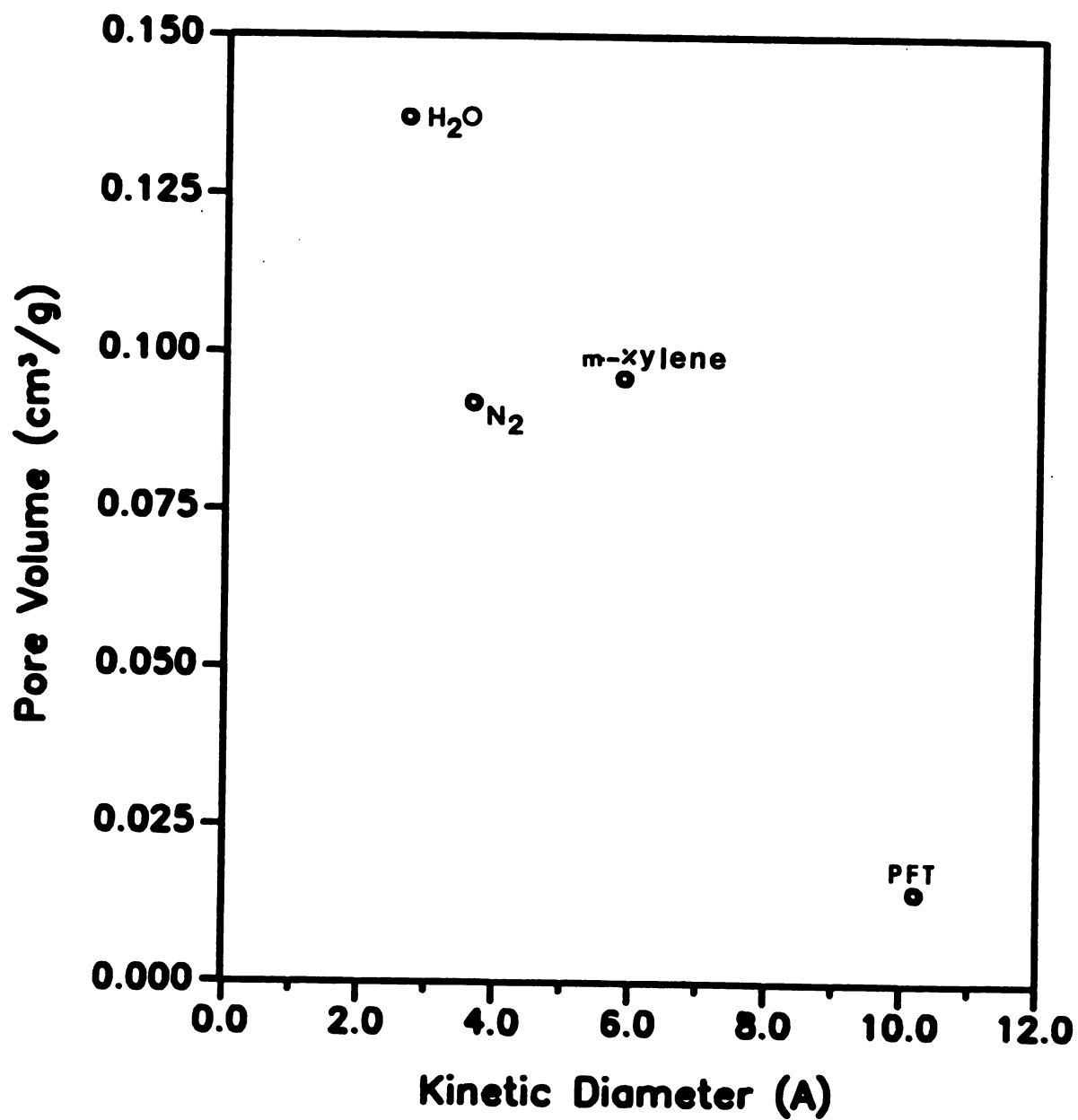
Figure II.20   Pore volumes for the TSLS complex based on
kinetic diameter of various molecules.

pH values[36]. Thus, the net positive charge carried by the tubes at ambient pH of the intercalation reaction (approx. 6.5) facilitates binding of the tubes to the negatively charged basal surfaces of exfoliated Na^+-montmorillonite in dilute aqueous suspension. Hydrogen-bonding between the outer Al-OH surface of the tubes and the siloxane oxygens of the smectite basal planes may also contribute to the intercalation process.

Although the tubes carry a net positive charge in aqueous suspension, the magnitude of the charge is insufficient to compensate completely for the negative charge on the smectite sheets. Thus, sodium ions are incorporated in the smectite galleries along with the imogolite tubes. The resulting cations exchange capacity (44.5 meq/100g) should make it possible to modify the surface acidity and catalytic properties of the TSLS complex by ion exchange with transition metal cations. The location of the cation in the galleries, whether bound to the smectite basal plane or to the imogolite surface, or both, remains to be determined.

It is important to point out several preferred experimental conditions for the successful synthesis of imogolite-smectite TSLS complexes. First the imogolite suspension must be dilute (approx. 1 wt%). Attempts to increase the concentration of imogolite solution to 2 wt% by evaporation led to self-aggregation and eventual flocculation of the tubes. The aggregated tubes could not

be redispersed or intercalated into the Na^+-montmorillonite. Secondly, the smectite clay must also be well-dispersed (exfoliated) in dilute aqueous suspension so as to optimize the accessibility of the basal surfaces. The layer charge density of the smectite may also be an important synthetic consideration. While montmorillonite with an average charge density of 0.6 e^- per $O_{20}(OH)_4$ unit cell is found to readily form a TSLS complex, we have not yet been successful in preparing a similar complex from fluorohectorite with a unit cell charge of $1.2e^-$. The higher charge density of the latter clay may limit the extent of layer delamination in aqueous suspension. The only d(001) x-ray diffraction patterns that were observed were those for the host clay, indicating that no intercalation product was formed.

The results of the X-ray diffraction patterns indicate that the imogolite tubes are indeed intercalated into the gallery regions of the host montmorillonite. This has been shown by the d(001) spacings of the X-ray diffraction patterns. The X-ray diffraction patterns taken at room temperature give a d(001) spacing of 34.8Å in accord with the van der Waals diameter of the imogolite tubes (23 Å) and the thickness of a montmorillonite layer (10 Å). The slight difference in the ideal value with the observed value may be attributed to adsorbed water in the interlayer region. Once the TSLS complex is heated to 100 °C the d(001) spacing is reduced to 32.9 Å which is in precise agreement with the expected value of 33 Å. In addition, the TSLS complex

exhibits a reasonably high degree of crystallinity at temperatures in excess of 500 °C. This result was interesting because although the TSLS complex remained moderately crystalline, there was a dramatic loss in surface area at temperatures above 400°C. This indicates that the tubes remain intercalated in the galleries of the host montmorillonite, but that the distortion of the tubes upon heating above 400°C is significant enough that the intratubular regions are no longer accessible by nitrogen. The fact that the surface area of the TSLS complex remains essentially unchanged to temperatures of 400°C is evidence that the imogolite is stabilized by intercalation. Pristine imogolite shows a dramatic loss in surface area at temperatures near 250°C. These results are consistent with the results which were obtained by FTIR of pure imogolite. Upon heating imogolite to a temperature of 200°C it was found that the tubes began to change in chemical composition. This change in chemical composition was accompanied by the loss of an infrared adsorption band at 995 cm^{-1} and the formation of a new SiOSi absorption band at 1090 cm^{-1} indicating that the imogolite tubes underwent a transannular condensation. Similar results have also recently been published by MacKenzie et al. They proposed two possible mechanisms for the collapse of imogolite based on ^{29}Si and ^{27}Al NMR. The first mechanism is given in Figure II.21 where the imgolite tube essentially cleaves and SiOH bonds condense across the tube to form SiOSi bonds.
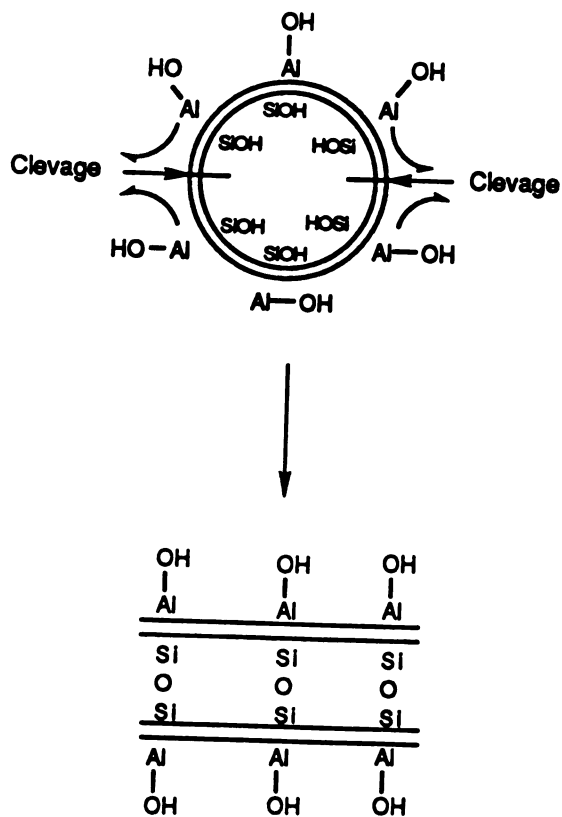
Figure II.21   Schematic diagram of a possible fracture
mechanism of imogolite showing SiOH-SiOH
condensation.

This mechanism is the prefered mechanism and is substantiated by infrared studies reported here· The second mechanism is given in Figure II.22 in which two imogolite tubes cleave outword and the outer AlOH bonds of one imogolite tube condense with the inner SiOH bonds of an adjacent tube to form an AlOSi bond. This mechanism seems to be disfavored because because for tube rupture to occur it is required that the AlOH bond be broken. Once this bond is broken the possibility that it would reform to condense with an SiOH group is unlikely. In addition, mechanism 2 seems even more unlikly to occur in the TSLS complex. For this type of cleavage to occur and the tube to unfold outward would require that the host clay layers would allow for the expansion of the imogolite. Based on this evidence the sequence shown in mechanism 1 is the only mechanism that seems realistic for the collapse of the imogolite tubes. This mechanism is also consistant with the XRD data and the surface area data at elevated temperatures.

^{29}Si MAS NMR results indicate that the intercalation of imogolite into the host layer of montmorillonite takes place with essentially no affect to the chemical composition or structure of the imogolite tubes. It has also been demonstrated that the imogolite tubes are preferentially exchanged over non imogolite moieties which are produced during the synthesis of the imogolite.

The NMR results also indicated that the imogolite tubes are clustered into specific domains which may contain areas
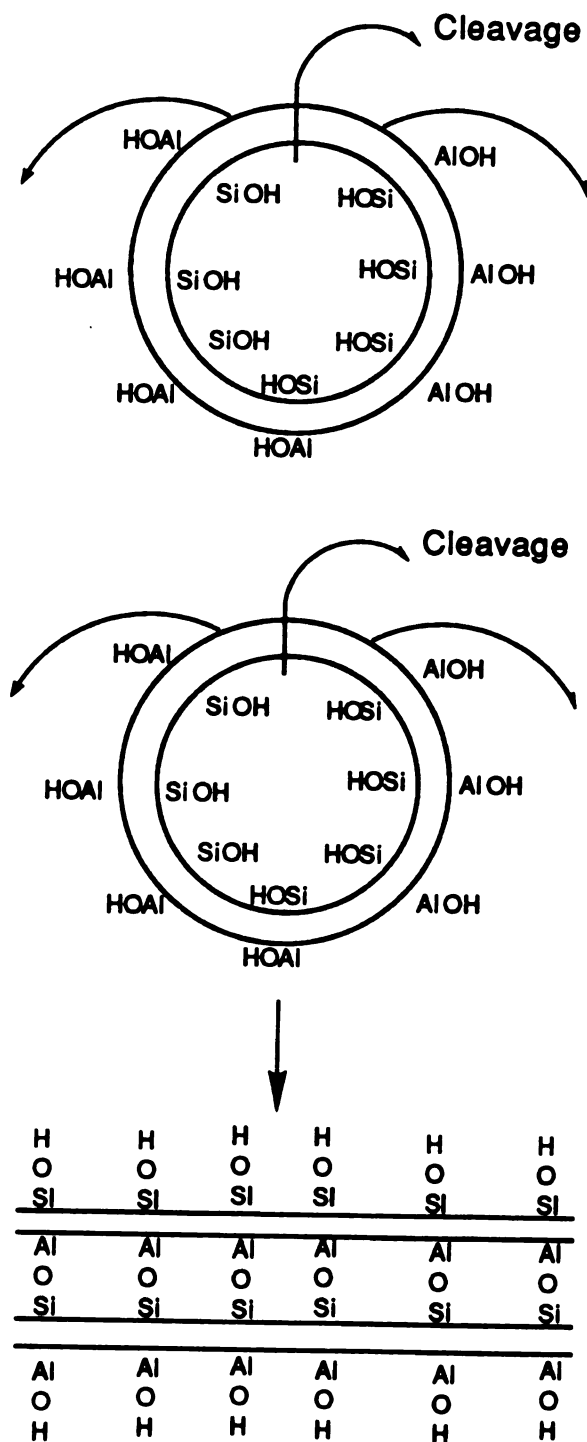
Figure II.22 Schematic diagram of a possible fracture
mechanism of imogolite showing SiOH-AlOH
condensation.

of mesoporosity and macroporosity. This was evidenced by the relative amounts of silicon attributed to the imogolite and montmorillonite in the TSLS complex. This indicated that approximately 46% of the theoretical surfaces of the montmorillonite sheets are occupied by imogolite.

Isotherms for the adsorption and desorption of nitrogen obtained for the TSLS complex indicated that at below P/P_0 =0.5 the shape of the adsorption isotherm is similar to a classical type I isotherm for microporous (<20Å) materials. Above P/P_0 of 0.5, tailing of the adsorption isotherm was observed due to meosporosity in the range 20-500Å. The presence of some mesopores was confirmed by the hysteresis loop observed upon desorption. The presence of mesoporosity indicates that the imogolite tubes are not perfectly ordered in the galleries of the montmorillonite. The proposed orientation of the imogolite tubes in the intergallery region can best be described as a log-jam type structure. The imogolite tubes are most likely randomly oriented or only partially aligned creating discreet domains of mesoporosity. The accessibility to the mesopores must then be through a network of intratubular imogolite channels.

The adsorption of nitrogen on the TSLS complex indicated a total liquid micropore volume of about 0.21 cm^3/g. This liquid pore volume is approximately one half of the liquid pore volume found for comparable zeolites such as zeolites 4A, X and Y which give pore volumes of 0.47, 0.51, and 0.48 cm^3/g respectively[22]. The TSLS complex affords the

adsorption of molecules with kinetic diameters as large as benzene (kinetic diameter 5.85 Å). Adsorption capabilities of the comparative zeolites afford adsorption of molecules with kinetic diameters of less than 3.8 Å for zeolite 4A and molecules with kinetic diameters of less than 8.1 Å for zeolites X and Y. These values indicate that the microporosity of the TSLS is very similar to that of a zeolite. The TSLS complex may then be thought of as essentially a two dimensional-zeolite.

LIST OF REFERENCES

1. Barrer, R. M.; McLeod, D. M. <u>Trans. Faraday Soc</u>. **1955**, *51*, 1290.

2. Vaughn, D. E. W.; Lussier, R. J. <u>Preprints 5th International Conference on Zeolites</u>; Naples, Italy, June 2-6, **1980**.

3. Pinnavaia, T. J. <u>Science</u> **1983**, *220*, 365.

4. Lahav, N.; Shani, V.; Shabtai, J. <u>Clays Clay Miner</u>. **1978**, *26*, 107.

5. Loeppert, R. H., Jr.; Mortland, M. M.; Pinnavaia, T. J. <u>Clays Clay Miner</u>. **1979**, *27*, 201.

6. Yamanaka, S.; Brindley, G. W. <u>Clays Clay Miner</u>. **1979**, *27*, 119.

7. Sterte, J.; Otterstedt, J. <u>Applied Cat</u>. **1988**, *38*, 131.

8. Adams, J. M. <u>Applied Clay Science</u> **1987**, *2*, 309.

9. Tilak, D.; Tennkoon, B.; Jones, W.; Thomas, J. M. <u>J. Chem. Soc., Faraday Trans</u>. **1986**, *82*, 3081.

10. Barrer, R. M. "Zeolites and Clay Minerals as Sorbents and Molecular Sieves." Academic Press: New York, 1978.

11. Pinnavaia, T.J.; Johnson, I.D., U.S. Patent 4,621,070, **1986**.

12. Lewis, R.M.; Van Santen, R.A., U.S. Patent 4,637,992, **1987**.

13. Occeli, M.L., in: "Proc. Intern. Clay Conf.",Denver, **1985**, ed. Schultz,L.G.; van Olphen, A.; Mumpton, F.A., Clay Minerals Society, Bloomington, **1987**, 319.

14. Yamanaka, S.;Nishihara, T.; Okumara, F.; Hattori, M., in: Abstracts, 24th Meeting Clay Miner. Soc., **1987**.

15. Moini, A.; Pinnavaia, T. J. Solid State Ionics, 1988, 26, 119.

16. Yoshinaga, N.; Aomine, S. Soil Plant Nutr. 1962, 8, 6.

17. Farmer, V. C.; Fraser, A. R. J. Chem. Soc., Chem. Commun. 1977, 32, 462.

18. Farmer, V. C.; Adams, M. J.; Fraser, A. R.; Palmieri, F. Clay Miner. 1983, 18, 459.

19. van der Gaast, S. J.; Wada, K.; Wada, S.-I.; Kukuto, Y. Clays Clay Miner. 1985, 33, 237.

20. Johnson, I. J.; Werpy, T. A.; Pinnavaia, T.J. J. Am. Chem. Soc., 1988, 110(25), 8545.

21. Pinnavaia, T.J.; et al., J. Mol. Cat. 1984, 27, 195.

22. Breck, D. W. "Zeolite Molecular Sieves" John Wiley and Sons, New York, 1974, 636.

23. Farmer, V.,C., U.S. Patent 4,252,779 1981.

24. Lippmaa, E.; Magi, M.; Samoson, A.; Engelhardt, G. and Grimmer, A.-R. J. Am. Chem. Soc. 1980, 102, 4889.

25. McKenzie, K. J. P.; Bowden, M. E.; Brown, I. W. N.; Meinhold, R.H. Clays and Clay Miner., 1989, 37(4), 317.

26. Russell, J.D.; McHardy, W.J.; Fraser, A.R. Clay Miner. 1969, 8, 87.

27. Brunauer, L.S.; Deming, L.S.; Deming, W.S.; Teller, E. J. Amer. Chem. Soc. 1940, 62, 1723.

28. Brunauer, L.S.; Emmett, D.H.; Teller, E. J. Amer. Chem. Soc. 1938, 60, 309.

29. Sing, K.S.W.; Everett, D.H.; Haril, R.A.W.; Moscou, L.; Pierotti, R.A.; Rouguerol, J.; Siemienewska, T. Pure and Applied Chemistry, 1985, 57, 603-619.

30. Dubinin, M.M. Pure and Applied Chemistry, 1965, 10, 309.

31. De Boer, J.M.; Lippens, B.C.; Linsen, B.G.; Broekhoff, J.C.P.; Van den Heuvel, A.; Osinga, Th. J. J. Coll. and Interface Sci., 1966, 21, 405-414.

32. Delon, J.F.; Dellyes, R. C.R.Ac.Sci. Paris, Serie D, 1967, 265, 1161-1164.

33. Greg, S.J.; Sing, K.S.W. in "Adsorption, Surface Area

and Porosity" Second Edition, **1982**, Academic Press, London.

34. Adams, M.J. J. Chromatog, **1980**, *188*, 231-234.

35. Wada, K.; Harward, M. E. Adv. Agron., **1969**, *26*, 211.

36. Farmer, V.C.; Adams, M.J.; Fraser, A.R.; Palmieri, F.Clay Miner. **1983**, *18*, 459.

CHAPTER III

Catalytic Properties of TSLS Complexes
Formed From Imogolite

3.1 Introduction

In recent years there has been a resurgence of interest in pillared clays containing metal oxide pillars[1-9] for applications in catalysis. The most important feature of these pillared clays is the increase in thermal stability to temperatures above 500°C[3]. The improved thermal stability has generated interest in using pillared clays as catalysts with possible applications in acid-catalyzed reactions.

This chapter will describe the acidity and catalytic properties of a new family of pillared clays in which a molecular-sized tubular aluminosilicate is intercalated in montmorillonite and beidellite. This family of pillared clays will be designated as tubular silicate-layered silicate(TSLS) intercalation compounds. Our interest in TSLS intercalation compounds stems from the unique structure of the tubular imogolite layered silicate. As was described in a previous paper[10] the accessible pore sizes of these materials is approximately 8.2Å making them interesting as potential shape selective catalysts.

The acidity of the TSLS complexes was investigated by FTIR studies of pyridine adsorption. The catalytic activity and selectivity was characterized by examining several model reactions. The reactions chosen were cumene cracking[11] as

a test for Bronsted acidity, m-xylene isomerization[12]as a test for selectivity and n-decane cracking[13] as a test for both acidity and selectivity.

3.2 Materials

The host clays used in this work were Na^+-montmorillonite and synthetic beidellite. The Wyoming Na^+-montmorillonite was obtained from the Source Clay Mineral Repository, University of Missouri Columbia Missouri. The Na^+-montmorillonite clay was purified by preparing a 2.5 wt.% aqueous suspension and allowing the coarse fraction to sediment over a period of 24 hrs. The suspended fraction was then collected, centrifuged, and treated at 70°C with an acetate-acetic acid buffer at pH 5.0 to remove calcium carbonate. Free non-lattice iron oxides were removed by treating the clay with 1.0M sodium carbonate, followed by subsequent treatment at 80°C with 1.0M sodium thiosulfite in the proportion 1 mL/g clay. Hydrogen peroxide (15 %) was used in the proportion 1 mL/g clay in a 1 wt. % suspension to remove organic impurities. The clay was then sodium saturated with 1.0 M NaCl. The flocculated particles were centrifuged and washed free of chloride ions. The final aqueous suspension was adjusted to a concentration of 1.0 wt. %. The unit cell formula of the montmorillonite was $Na_{(0.60)}$ $[Al_{3.23}$ $Fe_{0.42}$ $Mg_{0.47}]$ $(Si_{7.88}$ $Al_{0.13})$ O_{20} $(OH)_4$[14].

The beidellite used was a synthetic beidellite with a cation exchange capacity of 120 meq/100g. The beidellite

was obtained from G. Poncelet, CNRS Orleaves, France and had a calculated unit cell formula of $Na_{0.9}(Al_{4.0})[Si_{7.1}Al_{0.9}]$.

3.3 Physical Measurements

A Rigaku rotating anode X-ray diffractometer with Cu-K$^-$ radiation was used to measure d(001) basal spacings. The samples were prepared for X-ray analysis by air-drying 1 mL of a 1 wt. % suspension of clay onto a glass slide. The results discussed in this chapter were for samples prepared and data collected at room temperature.

Nitrogen Adsorption capacities for BET surface area measurements were determined at liquid nitrogen temperature on a Quantachrome Quantasorb Jr. using nitrogen as an adsorbate and helium as the carrier gas. The three-point BET method was used to determine surface areas. All of the samples were outgassed by heating under vacuum for 4 hours at 350°C.

Infrared spectra were collected on an IBM IR44 FTIR with a resolution of 2 cm^{-1}. All samples were prepared by air-drying approximately 1mL of a 1 wt.% suspension of the appropriate sample onto a silicon wafer.

The samples were then placed in a high temperature FTIR cell where they were outgassed under a low flow rate of helium to enhance heat transfer and reduced pressure for 4 hours prior to pyridine adsorption. Background samples were collected at various temperatures with the cell and silicon wafer in place. These spectra were saved and subtracted

from the actual sample spectra. The pyridine was allowed to adsorb onto the sample for a period of about 4 hours. The physically adsorbed pyridine was then removed by vacuum for a period of about 2 hours before the samples were heated. All of the spectra were collected while the sample was at the indicated temperature.

Catalysis results were obtained from a fixed bed reactor which had direct on line injection capabilities. All of the lines in the reactor were heated to assure complete vaporization of reactants and products. The reactor was connected directly to an HP-5890 G.C. fitted with a 60 m widebore Supelco SPB-1 column. Analytical grade standards were used to identify and quantitate peak location and areas.

3.4 Synthesis

The synthesis of the imogolite intercalated montmorillonite was accomplished by the reaction of the Na^+ exchange form of the clay with imogolite on a 2:1 wt/wt basis. The concentration of the Na^+-montmorillonite was 1 wt. % and the concentration of the imogolite was 0.9 wt. %. The imogolite was added dropwise to the stirred Na^+-montmorillonite suspension. The reaction was allowed to proceed at room temperature for 4 hours. The resulting complex was then washed thoroughly by centrifugation until the presence of imogolite was no longer detected. The presence of imogolite was indicated by the formation of a

colorless gel upon the addition of ammonium hydroxide. Once the sample has been washed free of imogolite it was air dried at room temperature.

The synthesis of the imogolite-intercalated beidellite required a larger amount of imogolite because of the higher cation exchange capacity. After several synthesis were tried it was determined that a weight ratio of 3:1 imogolite to beidellite was the most productive in giving a well ordered imogolite-beidellite complex. Higher concentration of imogolite gave similar X-ray diffraction patterns, and the need for the additional imogolite appeared to be unnecessary. The products formed using lower concentrations of imogolite were poorly ordered systems, and they were judged to be only partially intercalated.

The Ce^{3+}-exchanged forms of the imogolite-intercalated montmorillonite and beidellite were synthesized by using the residual sodium capacities as a guidline for the required amount of Ce^{3+}. As was stated previously, the imogolite intercalated montmorillonite exhibited a residual exchange capacity of 44.5 meq/100g of air dried sample indicating the surface charge of the imogolite could not fully compensate the layer charge of the host clay. It was also demonstrated by ^{29}Si MAS NMR that the actual composition of imogolite to clay in the montmorillonite complex was 0.36:1.0. Based on the van der Waals diameter of imogolite (23Å) and the unit cell size of montmorillonite the expected composition for complete monolayer coverage of the imogolite tubes would be

0.85:1. Thus, approximately 46 % of the interlayer space of the TSLS complex is occupied by imogolite. This unoccupied area is most probably the location of the residual sodium ions. The amount of Ce^{3+} used to exchange these materials was based on these results. The amount of Ce^{3+} added to the suspended imogolite montmorillonite and beidellite samples was based on a ten-fold excess of Ce^{3+} to the residual cation exchange capacity of the host TSLS complex. In the case of the imogolite intercalated montmorillonite an amount equivalent to 355 meq/100 grams of the TSLS complex was used and for the imogolite intercalated beidellite an amount equivalent to 850 meq/100 g of TSLS beidellite was used. These exchange reactions were allowed to proceed for four hours and then washed by centrifugation until free of excess Ce^{3+}. The samples were then air dried at room temperature. The Ce^{3+} clays were prepared in an attempt to increase acidity of the TSLS complexes. It has been demonstrated in several zeolitic systems that Ce^{3+} can improve the catalyst performance by either increasing acidity or decreasing coke formation on the catalyst.

The alumina pillared montmorillonite (APM) was prepared from a 50% wt/wt chlorohydrol solution obtained from Reheis Chemical Company. The alumina chlorohydrol solution used in this work was diluted from 6.2 M (as supplied) to 2.3 M. The diluted solution was then ion exchanged with the Na^+ form of the montmorillonite for four hours while stirring. The APM was then collected by centrifugation and washed four

times with water to remove any excess ACH. The material was then air dried on glass at room temperature.

3.5 Results

The TSLS complexes were characterized by X-ray diffraction and surface area measurements. The X-ray diffraction patterns for the various TSLS complexes are given in Figures III.1 and III.2. Figure III.1 is a representative X-ray diffraction pattern for TSLS(mont) andTSLS(Ce $^{3+}$ mont). The TSLS(mont) gives a first order reflection at 38.4Å, a second order reflection at 19.3Å, and a third order reflection that appears as a shoulder at 12.8Å. The TSLS(Ce^{3+} mont) gives a first order reflection of 34.2,Å a second order reflection at 17.2Å, and a third order reflection that appears as a shoulder at 11.5Å. This difference in d-spacings may be attributed to different amounts of water in the interlayer or the difference in hydration energies of the interlayer cations. The Ce^{3+} may coordinate the water more tightly than the imogolite tubes. There is also a difference in the relative intensities of the first and second order peaks between the TSLS(mont) and the TSLS(Ce^{3+} mont) due to the differences in scattering power of the intergallery region.

Figure III.2 shows the X-ray diffraction patterns for the TSLS(beid) and the TSLS(Ce^{3+}beid). The first order reflection for the TSLS(beid) occurs at 39.7Å, the second order reflection occurs at 20.4Å, and a third order
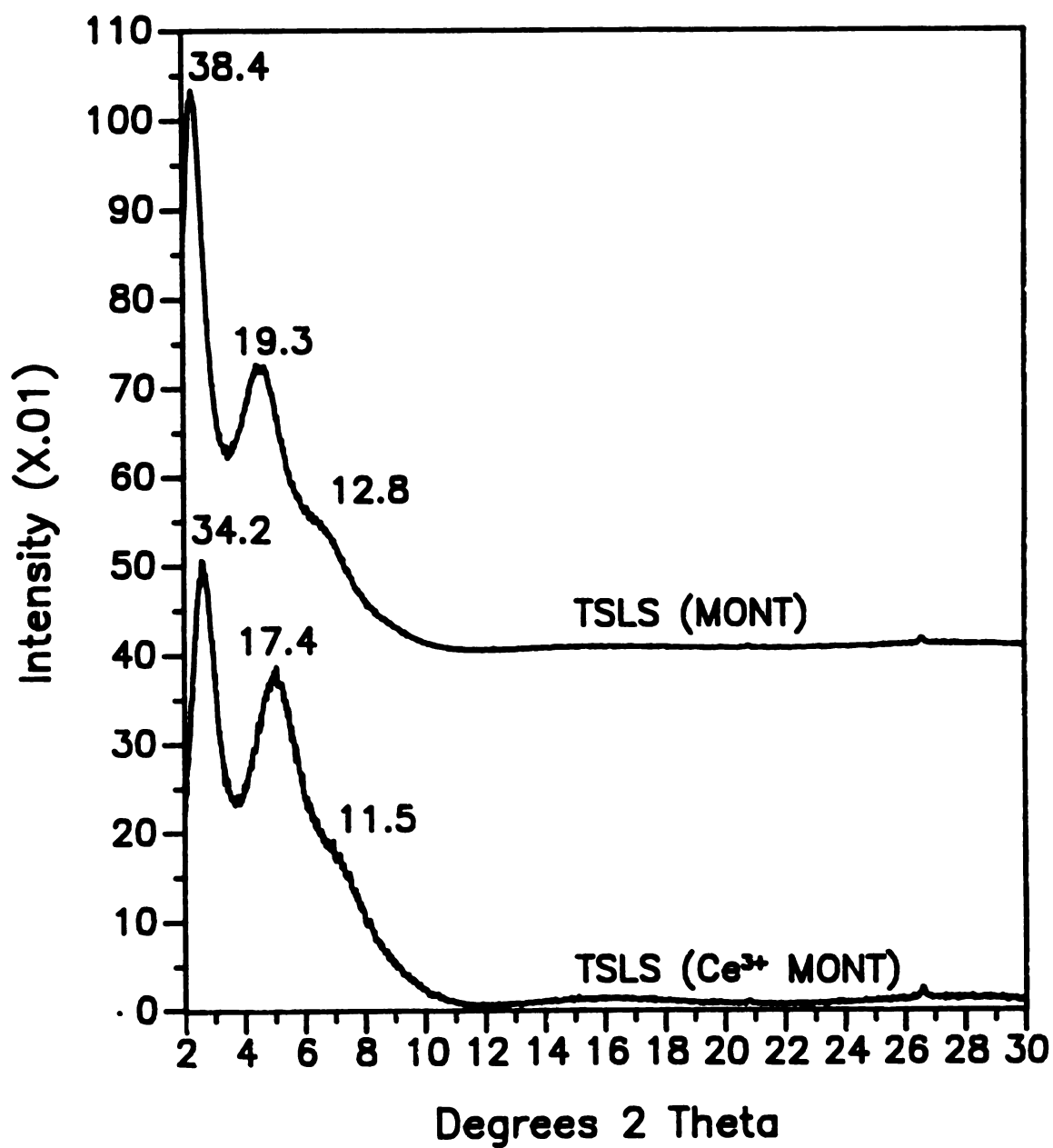
Figure III.1   X-ray diffraction patterns of TSLS(mont) and TSLS(Ce^{3+}-mont) air dried at room temperature.
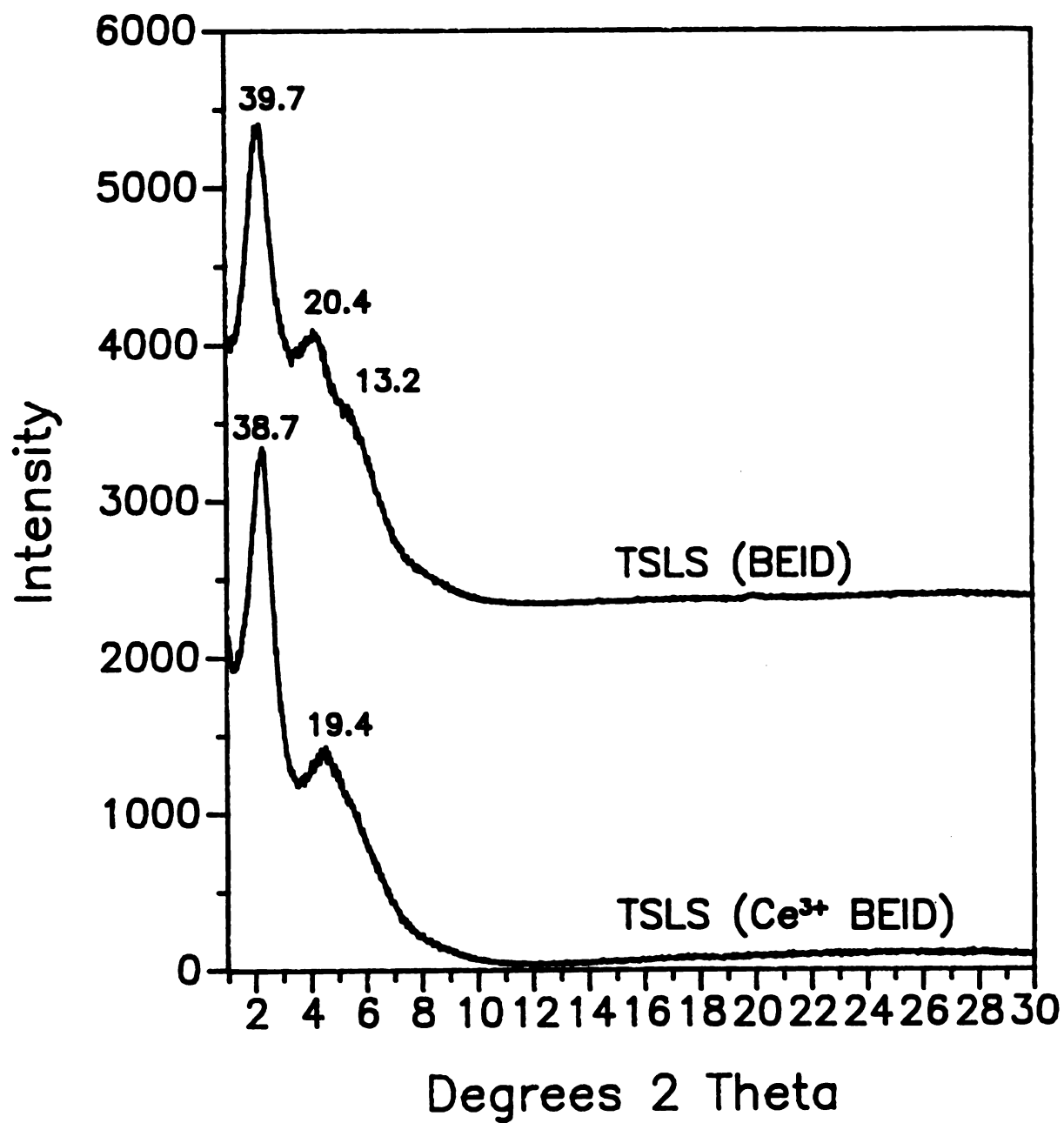
Figure III.2   X-ray diffraction patterns of TSLS(beid) and TSLS(Ce^{3+}-beid) air dried at room temperature.

reflection that appears as a shoulder at 13.2Å. The relative intensities between the first and second order peaks differ between the TSLS(beid) and the TSLS(Ce^{3+}-beid) because of the relative scattering power of the interlayer cations. The low number of 001 reflections in all of the X-ray diffraction patterns indicate that these materials show moderate order along the c-axis, in addition to being turbostatic in the ab plane.

The APM x-ray diffraction pattern gave several orders of $d_{(ool)}$ reflections. The first order reflection yielded a d-spacing of 18.6 Å. The second order reflection was at 9.3 Å. The x-ray diffraction pattern gave six rational orders of $d_{(ool)}$ reflections.

The amount of Ce^{3+} contained in the TSLS(mont) sample was equal to 0.15 g Ce^{3+} per 100 g of sample. The amount of Ce^{3+} contained in the TSLS(Beid) was 0.80 g per 100 g of complex. These differences may be attributed to the different cation exchange capacities of the host clays or due to the differences in location of the charge. The beidelite complex appears to have a higher affinity for the Ce^{3+} than the montmorillonite complex based on these results.

The BET nitrogen surface areas for the TSLS complexes when outgassed under vacuum for four hours at 350°C are as follows: TSLS(mont)=375 m^2/g $\pm$ 15 m^2/g, TSLS (Ce^{3+}-mont) = 262 m^2/g $\pm$ 13 m^2/g, TSLS(beid) = 320 $\pm$ 15 m^2/g, and TSLS(Ce^{3+}-beid) = 280 m^2/g $\pm$ 23 m^2/g. All of the BET

surface areas are very similar, indicating that the adsorption is probably taking place on the inner surfaces of the imogolite tubes. The surface area of the reference alumina pillared montmorillonite is 284 $\pm$ 18 m^2/g. The similarities in surface area among the TSLS complexes is somewhat interesting because elemental analysis indicates that there is approximately 10% more imogolite by weight in the TSLS(beid) than the TSLS(mont). This would indicate that the surface area should be higher in the TSLS(beid) than the TSLS(mont). The differences in surface areas however, is dependent on accessibility of the adsorbate to the internal channels of the tubes. Intergallery ordering of imogolite may be different between the two host clays because of the difference in cation exchange capacities and charge location. This difference in intergallery ordering may account for the differences in surface areas. In addition, the thermal stability of all the samples is equivalent at least to 350°C.

3.6 Surface Acidity

Acidity in pillared clays may be generated in different ways. One source of acidity may come from the polarization of water molecules by charged cations in the interlayer region. A higher charge to radius ratio will have a greater polarizing affect on the water molecule and will lead to increased acidity. This type of acidity appears to occur at lower temperatures when there is still water associated with

the interlayer region. A second source of acidity can be generated by the host clay layer. In the case of beidellite pillared clays protons can be bound to the $Si^{IV}OAl^{III}$ linkages in the tetrahedral layer generating $Si^{IV}OHAl^{III}$ linkages. This type of bonding is also found in many zeolites like zeolite Y^{13}. These types of bonding arrangements are found in beidellite because of the substitution of Al for Si in the tetrahedral layers. In the case of montmorillonite this does not happen because the substitution occurs in the octahedral layer with Mg replacing Al. A third type of acidity can be generated in pillared clays by the pillar itself as is the case with the aluminum pillared smectites. Upon dehydration/ dehydroxylation of the $Al_{13}O_4(OH)_{24}(H_2O)_{12}^{7+}$, Kegin ion, up to seven protons can be liberated generating Bronsted acidity.

FTIR spectroscopic studies of pyridine adsorbed on the surface of TSLS(mont) and TSLS(beid) was used to identify the nature and strength of the acid sites. This adsorbate is known to exhibit aromatic ring stretching frequencies characteristic of pyridinium ion (Bronsted acidity) and can be seen by an absorption band at 1450 cm^{-1}. Coordinated pyridine molecules (Lewis acidity) is evidenced by an absorption band at 1490 cm^{-1}. An absorption band near 1490 is indicative of ring stretching and is assigned to both Bronsted and Lewis acidity[15,16].

Figure III.3 shows the FTIR spectra of pyridine

Figure III.3   FTIR spectra of pyridine adsorbed on TSLS
(mont) at room temperature and heated to the
corresponding temperatures under reduced
pressure and a low flow of helium. Samples
were prepared by air drying 1 mL of a 1 wt %
suspension onto a silicon wafer and pre-
treating at 350°C under reduced pressure and
a low flow of helium.

adsorbed on TSLS(mont). The absorption due to pyridine bound to Lewis sites at 1450 cm^{-1} is very intense. The presence of Bronsted acidity is indicated by the very weak absorption band at 1540 cm^{-1} of the pryidinium ion. There is also a moderate band at 1490 cm^{-1} which is attributed to both Bronsted and Lewis acidity. The bands at 1490 cm^{-1} and 1440 cm^{-1} decrease rapidly as the temperature is increased, giving an indication that many of the acid sites present arerelatively weak. Lewis acidity is still present even to temperatures of 400°C. The fact that the TSLS(mont) shows very little Bronsted acidity at higher temperatures leaves some question as to how effective it will be as an acid catalyst.

Figure III.4 is the FTIR spectra of pyridine adsorbed on TSLS(beid) pretreated at 350°C. There is a substantial difference in the amount of Bronsted acidity between the TSLS(beid) and the TSLS(mont). The TSLS(beid) shows a substantial increase in Bronsted acidity over the TSLS(mont). An approximate integration of the absorption bands assigned to Bronsted acidity shows that the TSLS(beid) exhibits three times as many Bronsted acid sites to the TSLS(mont). In addition, since the integrated area of the Lewis band at 1440 cm^{-1} is nearly equivalent in intensity in both TSLS complexes, the increase in this ratio must therefore be due to an increase in the number of Bronsted acid sites.

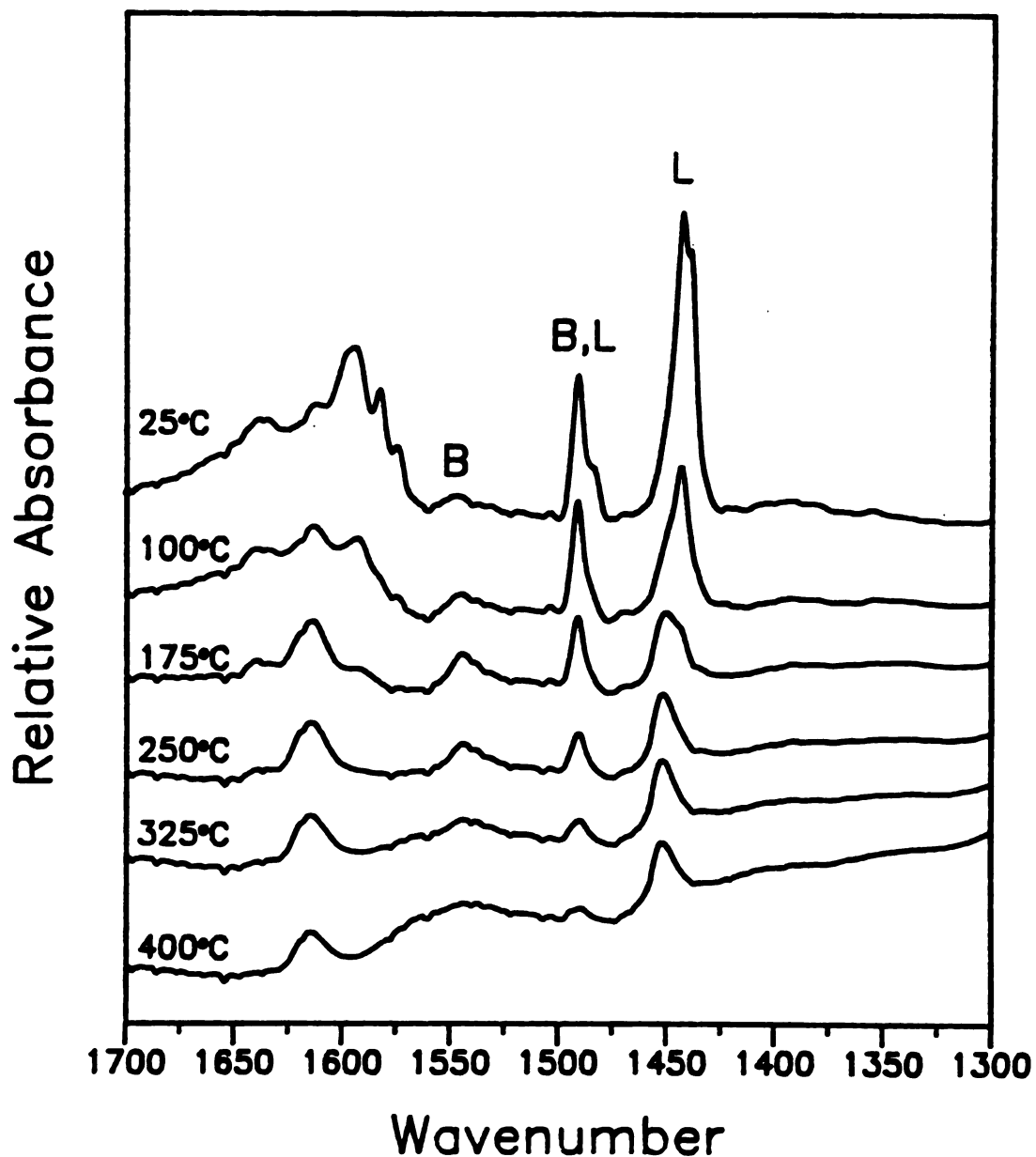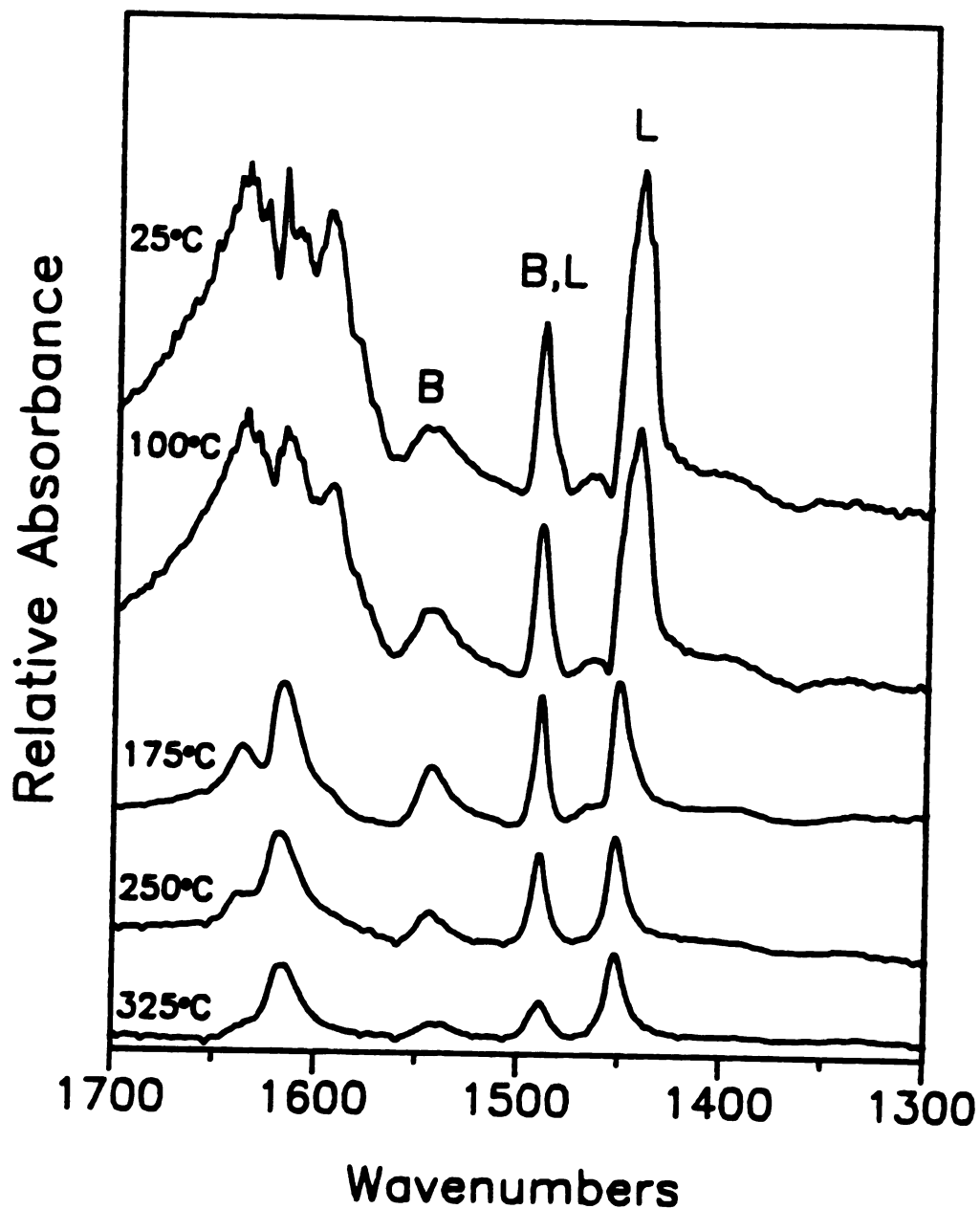The difference in acidity between the TSLS(beid) and

Figure III.4   FTIR spectra of pyridine adsorbed on TSLS
(beid) at room temperature and heated to the
corresponding temperatures under reduced
pressure and a low flow of helium. Samples
were prepared by air drying 1 mL of a 1 wt %
suspension onto a silicon wafer and pre-
treating at 350°C under reduced pressure and
a low flow of helium.

the TSLS(mont) can be attributed to the difference in the host clay since the intercalated cation(imogolite) is identical in both materials. This increase in acidity can be illustrated in Figure III.5[13].

In beidellite the substitution of Al for Si in the tetrahedral sheet creates SiOAl bond linkages in which the aluminum carries a net negative charge. This negative charge may then be compensated by a proton. This proton may be contributed to the clay layer of beidellite by theimogolite tube or by interlayer water which has disassociated. This proton donation is one plausible reason for the increase in Bronsted acidity for the TSLS(beid) over the TSLS(mont). As a preliminary conclusion, the TSLS(beid) should offer better activity as an acid catalyst than the TSLS(mont)(based on acidity measurements).

The acidity of the APM has been shown by Ocelli et. al. to be significant in both Lewis and Bronsted sites. Acidity in these materials persists to temperatures above 500°C, as shown by pyridine adsorption. At these elevated temperatures most of the acidity is of the Lewis type[17].

3.7 Cumene Cracking

Cumene cracking was used as a model reaction for the further elucidation of Bronsted acidity in the pillared TSLS complexes. The mechanism for this reaction is given in Figure III.6. This reaction was selected for study because the mechanism is well understood to be Bronsted acid
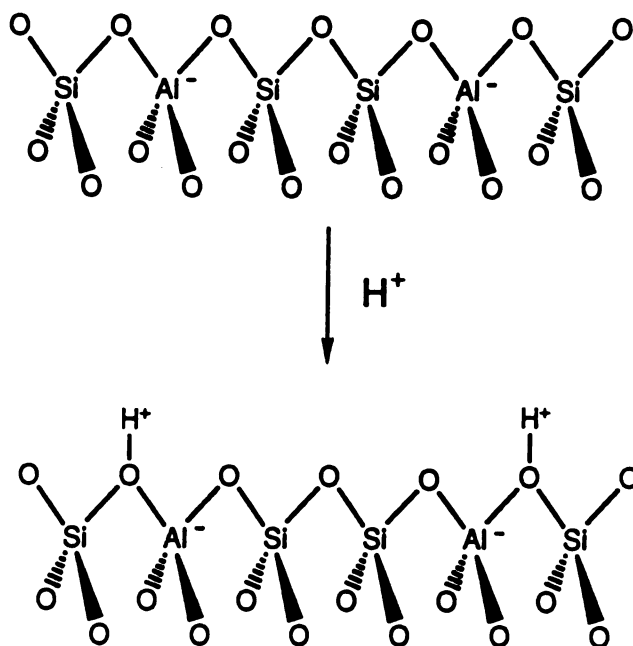
Figure III.5   Schematic representation of the mechanism
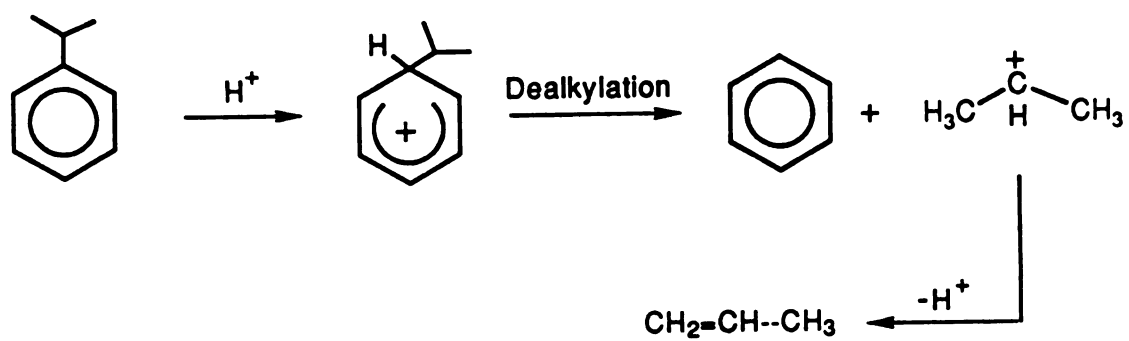for the generation of acid sites in
beidellite.

Figure III.6   Reaction mechanism of cumene cracking
                showing dealkylation to benzene and
                propylene.

catalyzed.[11] In addition, there are very few sidereactions, which means that the major products are benzene and propylene.

Figure III.7 shows the percent conversion of cumene to benzene as a function of time on stream. The initial reactivities after five minutes of reaction done were in the order TSLS(Ce^{3+}-beid) > TSLS(beid) > APM > TSLS(Ce^{3+}-mont) > TSLS(mont). It is interesting to note that the initial reactivities do not follow the BET surface areas indicatingthat intrinsic differences in acidity influence reactivity. The TSLS(Ce^{3+}-mont) which is not shown in Figure III.7, showed a conversion of less than 30%. After the reaction was allowed to proceed for longer periods of time the order of activity changed as follows: TSLS(beid) > TSLS(Ce^{3+}-beid) > APM > TSLS(mont). The differences between the initial activities and the final activities shows that the TSLS(beid) maintains its catalytic activity longer than the other catalysts. When comparing the TSLS(beid) to the standard (APM) catalyst the differences in initial activities is approximately 2%, conversion. However the difference in final activities is 15% conversion with the TSLS(beid) maintaining the highest activity. This difference in activities as a function of time indicates that the TSLS(beid) is less susceptible to coke formation than the APM and, in fact, to all of the other catalysts tested. Analysis of the % carbon after 25 minutes on stream showed that indeed coke formation for the TSLS (beid) was
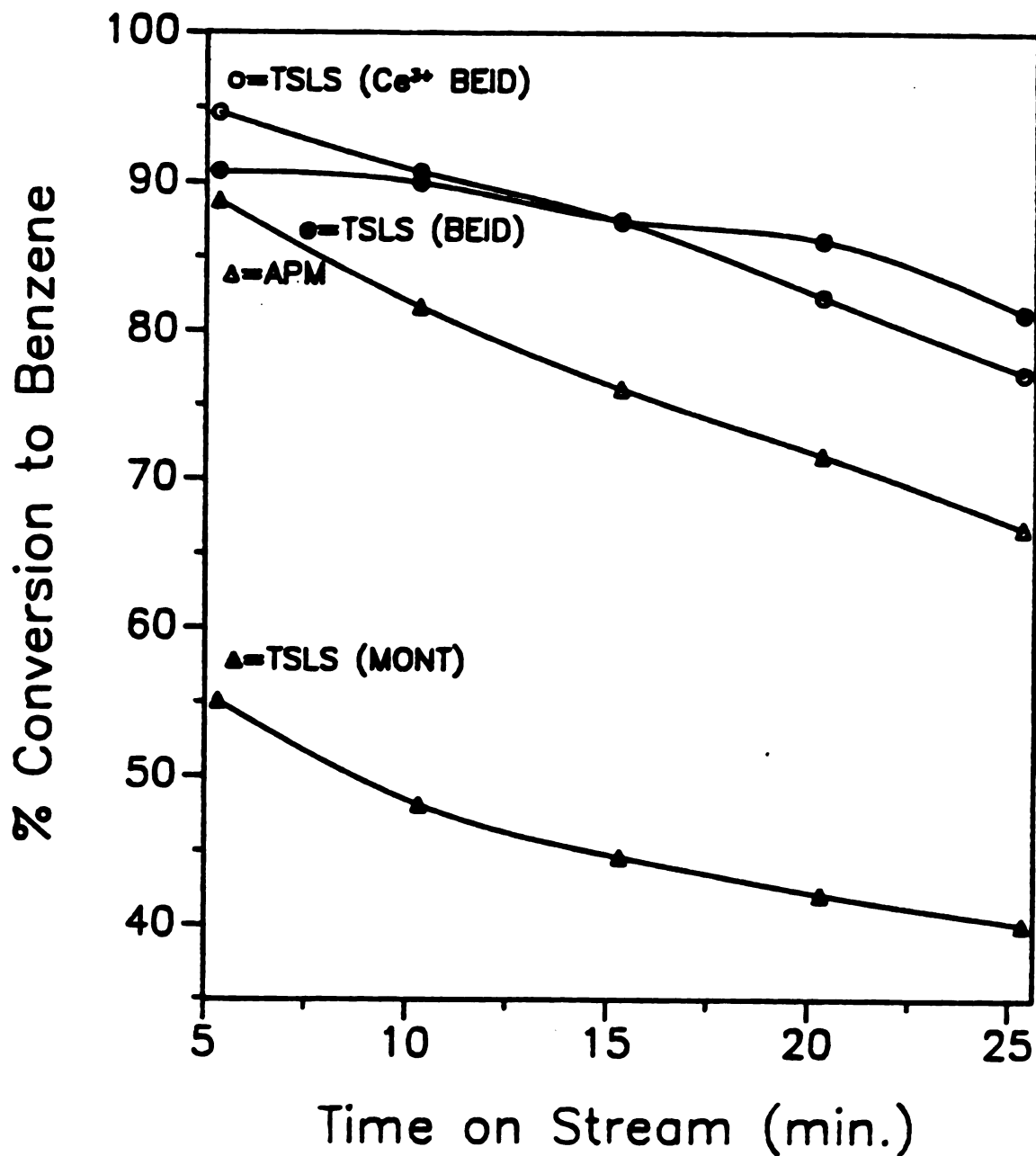
Figure III.7   Conversion of cumene over various TSLS
complexes and alumina pillare montmorillonite.
Reaction conditions: Temperature = 350°C;
WHSV = 0.4 g cumene per gram of catalyst per
hour; contact time = 1.5 seconds.

less than 4% by weight while the other catalysts had cokeformations of slightly over 6%.

The higher activity for the TSLS(beid) over the TSLS(mont) is in agreement with the previous results of the FTIR studies of pyridine adsorbed on the surfaces of these complexes. The similarity in the activity between the TSLS(beid) and the APM must be attributed to the pillars in the interlayer. The Al_{13} pillar has been shown to generate Bronsted acidity upon dehydration/dehydroxylation upon calcination at elevated temperatures[17,18]. The TSLS(beid) exhibited the best conversion and the lowest deactivation as a function of time of all the catalysts tested.

The samples which contained cerium did not show any enhanced activity. This is somewhat surprising since in many zeolitic systems cerium is used as a promoter to either enhance acidity or reduce coking. This indicates that the cerium must act in a different manner in the TSLS complexes than it does in the zeolitic systems.

3.8 m-Xylene Isomerization

The second reaction that was examined was the isomerization of m-xylene to o-xylene and p-xylene. This reaction was used to investigate pore sizes based on the selectivity to ortho and para xylene as opposed to dealkylated or transalkylated products. The percent isomerization was defined by %p-xylene + % o-xylene / % conversion to all products. The mechanism for the
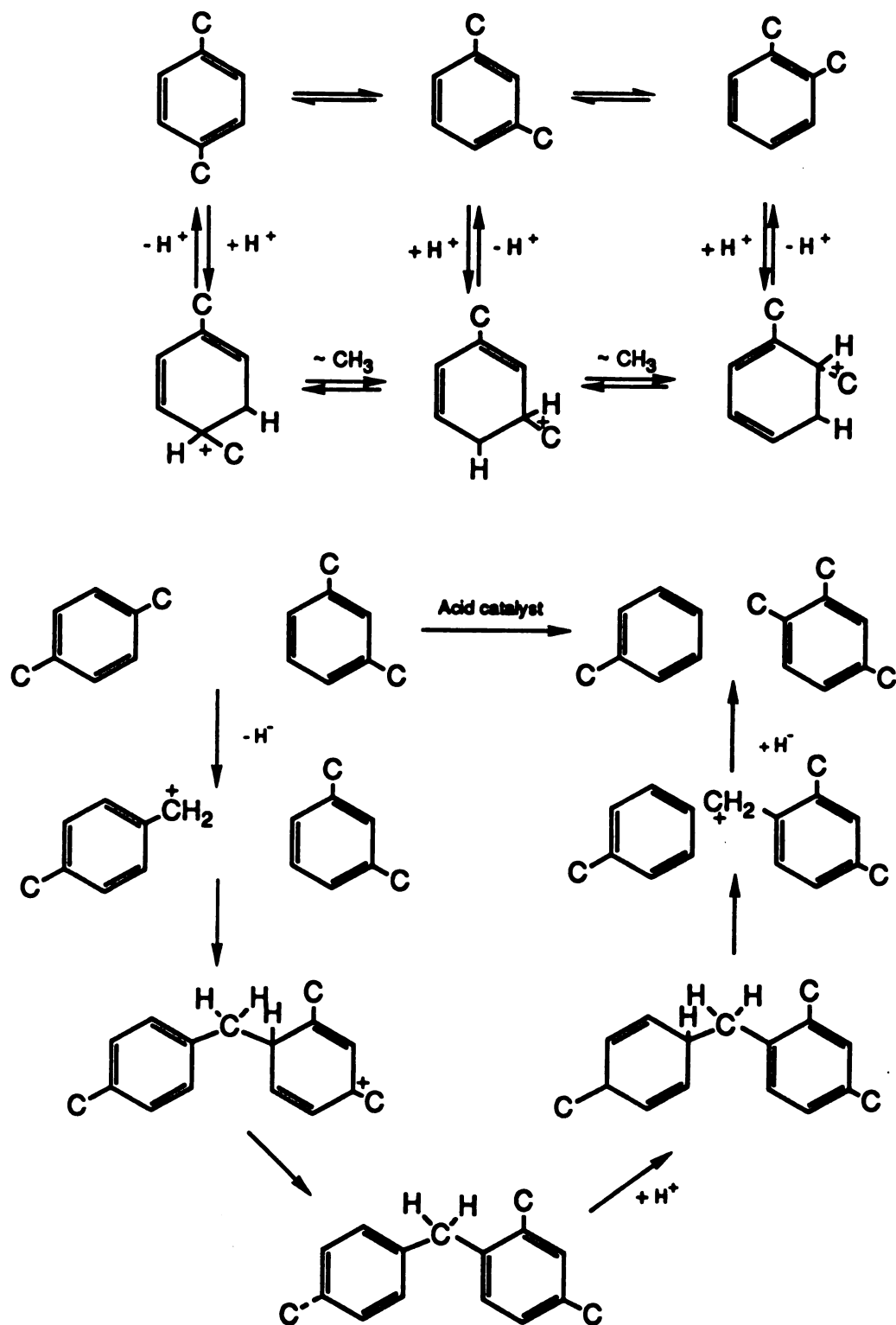
Figure III.8   Mechanism for the isomerization and for the dealkylation of m-xylene to various isomers and transalkylated products.

isomerization of m-xylene is given in Figure III.8. Figure III.9 shows the percent total conversion of m-xylene as a function of time. The initial conversion shows the following order of activity: APM > TSLS(Ce^{3+}-beid) > TSLS(beid) > TSLS(mont). The order of activity after 25 minutes on stream is TSLS(beid) > TSLS(Ce^{3+}-beid) > APM > TSLS(mont). The order of deactivation for m-xylene isomerization is then APM > TSLS(Ce^{3+}-beid) > TSLS(Ce^{3+}-mont) > TSLS(beid). The deactivation indicates that the TSLS(beid) is again less susceptible to coke formation than that of the other catalysts tested.

The selectivity to isomerized products, dealkylated products and transalkylated products is given in Table III.1. The most striking feature regarding selectivity is the high selectivity toward isomerized products for TSLS(beid). The TSLS(beid) yields a selectivity to isomerized products selectivity of 89.4%, while the TSLS(mont) gives only 52.4% and the APM gives 41.2%. The high isomerization selectivity for the TSLS(beid) may indicate that the isomerization is taking place on the internal channels of the imogolite tubes. This is plausible because the intermediates necessary for the formation of the transalkylated products require the combination of two m-xylene molecules to come together and react[11]. The internal dimensions of the imogolite tubes (approx. 8Å) would disfavor bimoleucular intermediates.
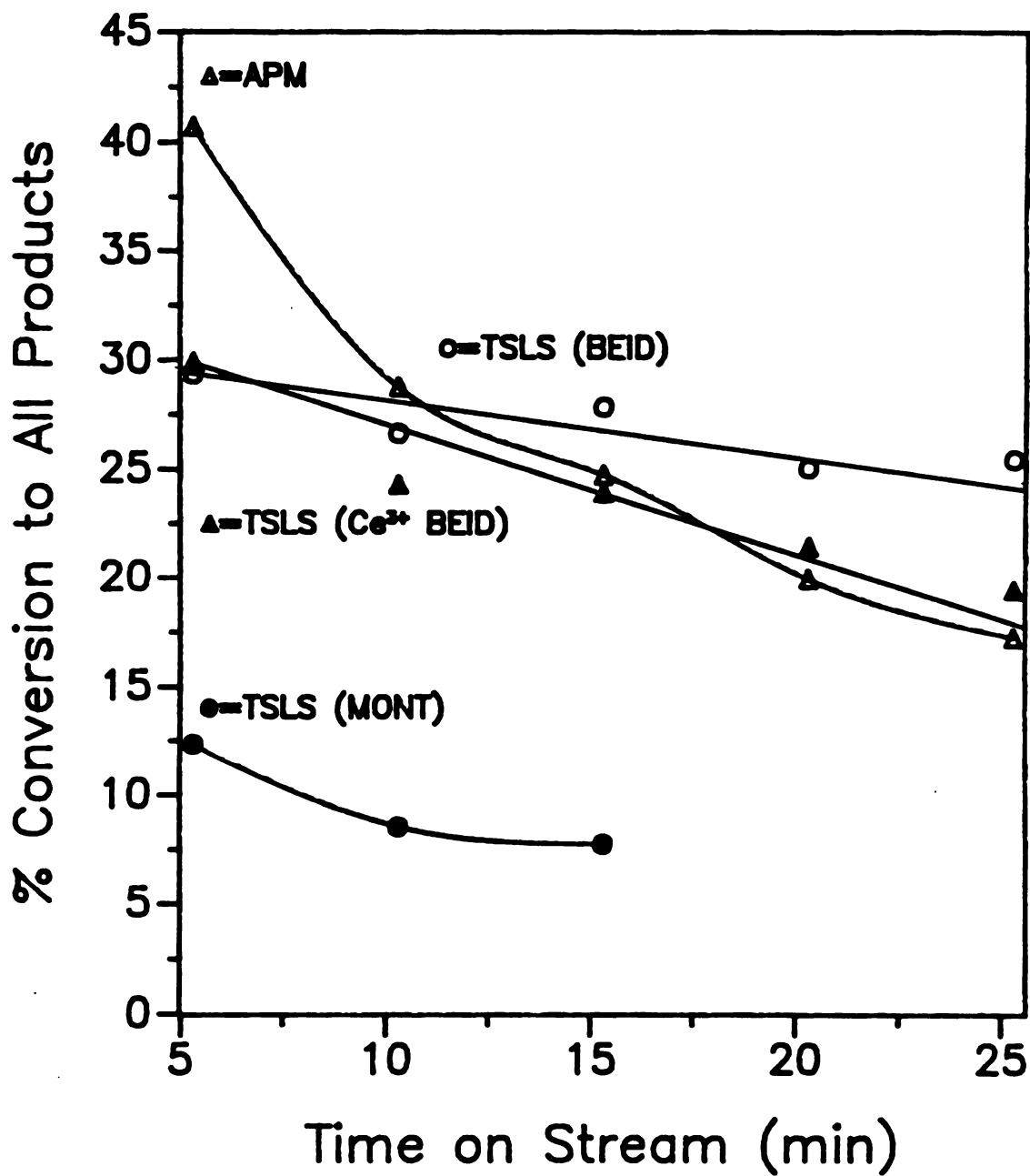
Figure III.9   Conversion of m-xylene isomerization over
                various TSLS complexes and alumina pillared
                montmorillonite. Reaction conditions:
                Temperature = 350°C; WHSV = 0.4 g cumene per
                gram of catalyst per hour; contact time = 1.5
                seconds.

Table III.1 Conversion of m-xylene over TSLS complexes and alumina pillared montmorillonite (APM)[a].

	APM	TSLS Mont.	TSLS Beid.
% Conversion	40.7%	12.4%	29.3%
% Isomerization	41.2%	52.4%	89.4%
% p-Xylene	17.2%	20.2%	44.0%
% o-Xylene	24.0%	32.2%	45.4%
p-xylene/o-xylene	0.71	0.62	0.97
% Dealkylation	30.4%	26.6%	6.8%
% Transalkylation	28.4%	21.0%	3.8%

[a] Reaction Conditions: Temperature = 350°C; WHSV = 0.4 g m-xylene per gram of catalyst per hour; contact time = 1.5 seconds.

The TSLS(mont) does not exhibit substantial isomerization. The Bronsted acidity in this case is low, and the reactions may be taking place on the external surfaces of the clay or at broken edge sites. These sites would permit bimolecular reaction intermediates to form. Hence transalkylation would be expected to compete favorably with isomerization.

As in the case of cumene cracking, the TSLS(beid) is less susceptible to deactivation compared to the other catalysts tested. Also, the TSLS(beid) shows a much higher selectivity to isomerized products and a higher ratio of para to ortho xylene. This latter results also would support intratubular reaction. However, TSLS (mont) also should exhibit intratubular reaction and corresponding high isomerization activity, but it does not. This may be attributed to a fewer number of acid sites present in the intratubular regions of the TSLS(mont). These acid sites are required for isomerization to take place.

3.9 Decane Cracking

The catalytic cracking of n-decane was used to obtain information about the strength of the Bronsted acid sites as well as information about pore sizes. The general mechanism for the conversion of paraffins to various products is listed illustrated in Figure III.10.

Figure III.11 shows the %total conversion of n-decane to all products as a function of time on stream. The

$$R\text{-}CH_2\text{-}CH_2\text{-}CH_2\text{-}CH_2\text{-}R^{'} \xrightarrow{\text{Catalyst/H}^+} R\text{-}CH_2\text{-}\overset{+}{C}H\text{-}CH_2\text{-}CH_2\text{-}CH_2\text{-}R^{'} + H_2$$

$$R\text{-}CH_2\text{-}\overset{+}{C}H\text{-}CH_2\text{-}CH_2\text{-}R^{'} \longrightarrow R\text{-}CH_2\text{-}CH{=}CH_2 + R^{'}\text{-}\overset{+}{C}H_2$$

$$R^{'}\text{-}CH_2^{+} + H_2 \longrightarrow R\text{-}CH_3 + H^{+}$$
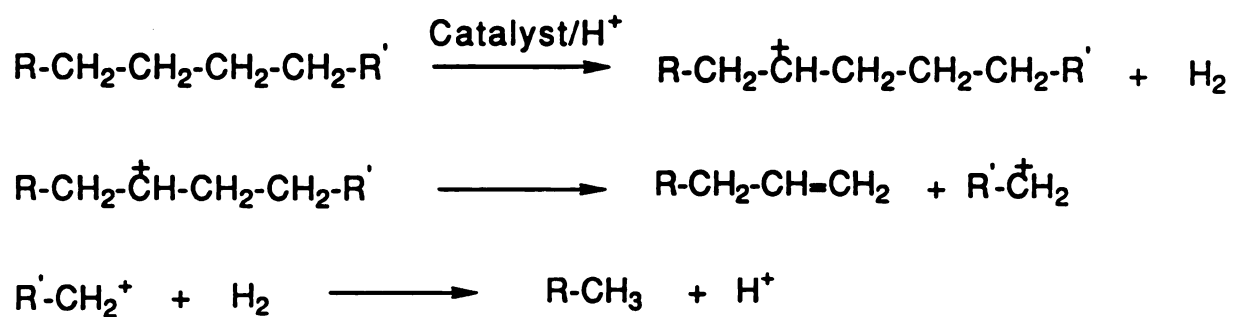
Figure III.10   General mechanism for the conversion of parffins to various cracked products.
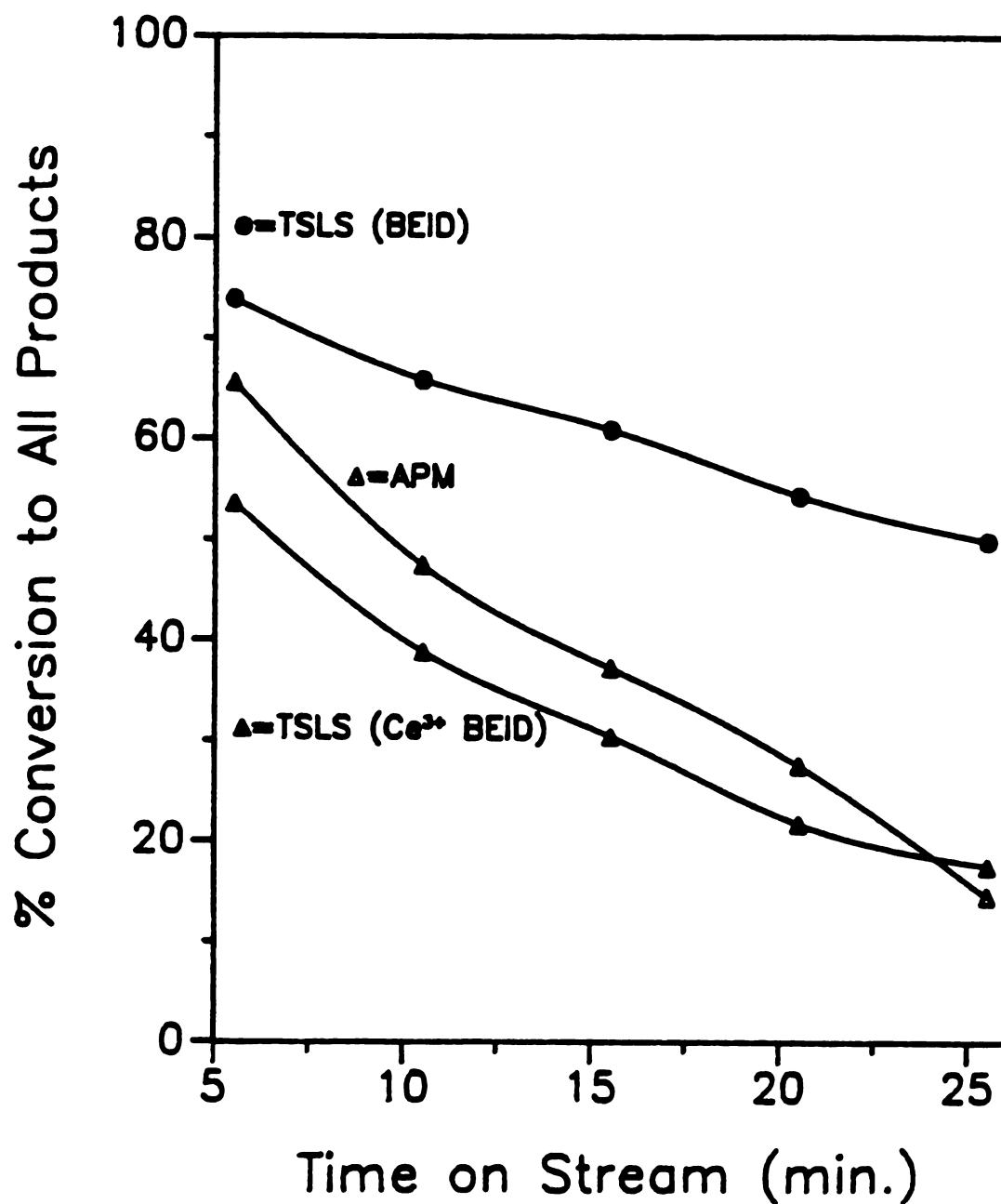
Figure III.11   Conversion of n-decane cracking over
                various TSLS complexes and alumina pillared
                montmorillonite. Reaction conditions:
                Temperature = 350°C; WHSV = 0.4 g cumene per
                gram of catalyst per hour; contact time = 1.5
                seconds.

initial activities are as follows TSLS(beid) > APM > TSLS(Ce^{3+}-beid). The TSLS(mont) and TSLS(Ce^{3+}-mont) complexes are not described because the conversion of these catalysts were both less than ten percent. After 25 minutes on stream the order of activity is TSLS(beid) > TSLS(Ce^{3+} beid) > APM. The rate of deactivation is APM > TSLS(Ce^{3+}-beid) > TSLS(beid). The TSLS(beid) shows a very high initial conversion of 78% indicating that the Bronsted acid sites that are present are of substantial strength and are stronger than the Bronsted acid sites present in TSLS(Ce^{3+}-beid) and APM.

The product distribution based on carbon number is given in Figure III.12. The majority of the products fall in the C_3-C_6 range. Although the distribution is similar there is a tendency for the APM to produce higher carbon number products than the TSLS complexes. This is due to the larger pores in the APM compared to the TSLS complexes·

The product distribution in the cracking of n-decane over zeolites behaves in a much different manner. The products obtained from the proton form of faujasite (HNaY) gave 45% C_3 and about 30% C_4 with the rest of the products being C_2, C_5 and C_6. Almost identical results are obtained with mordenite, another large pore zeolite. The product distribution shifted only slightly to higher amounts of C_3 when a medium pore ZSM5 zeolite was used[19]. These results indicate that the TSLS complexes contain larger, less tortuous pores than many commercial zeolites. This
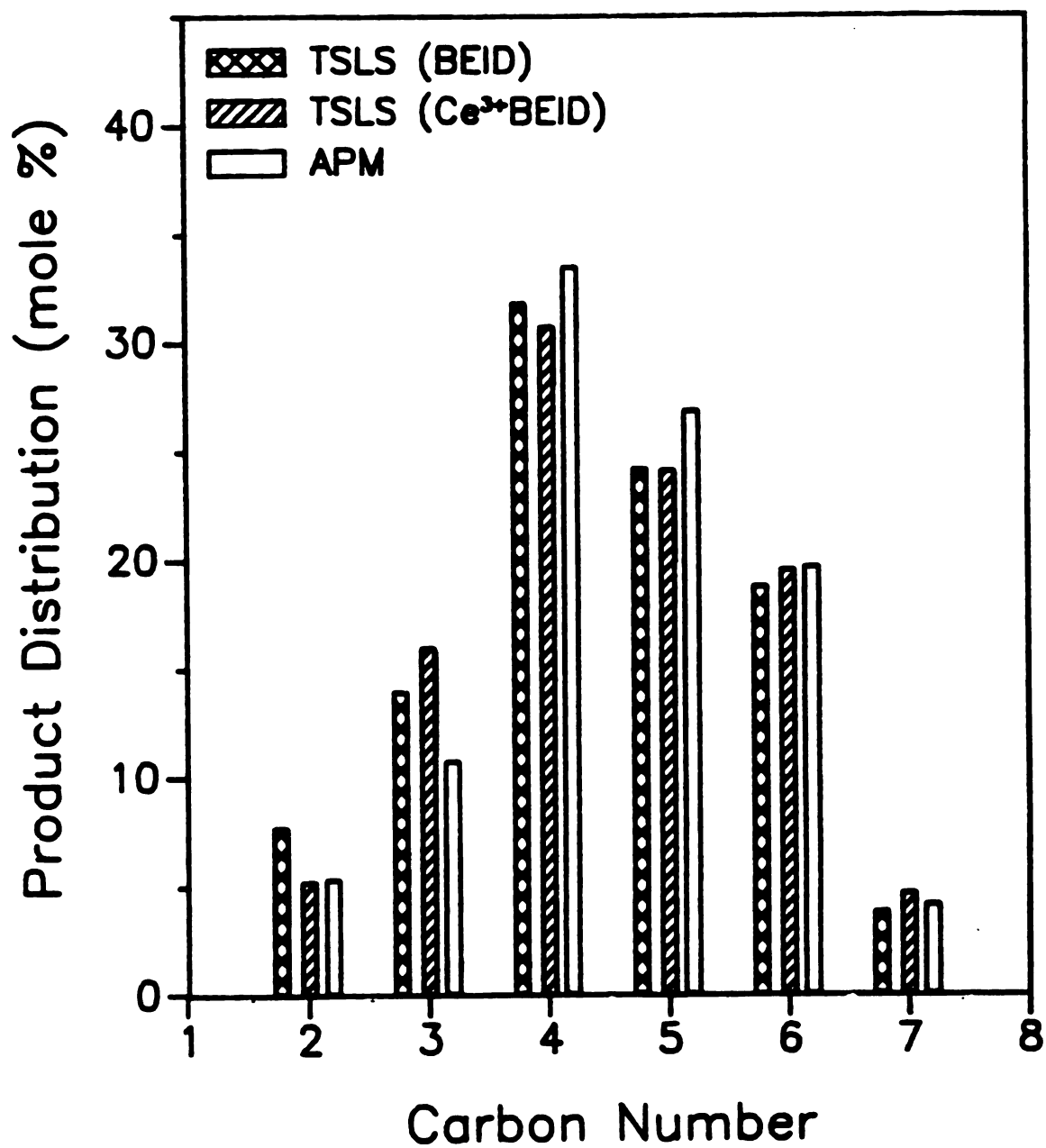
Figure III.12   Product distribution of n-decane cracking over various TSLS complexes and alumina pillared montmorillonite.

difference could potentially be used in the cracking of heavier feedstocks of oil where the elimination of light gas products is highly desirable.

The conversion of decane is best facilitated by the TSLS(beid). This complex also shows a high selectivity to products in the C_4-C_6 range.

3.10 Conclusions

The synthesis of TSLS complexes by intercalation of imogolite into montmorillonite and beidellite has been clearly demonstrated by X-ray diffraction and surface are measurements. The X-ray diffraction patterns indicated relatively well ordered layered materials with d spacings on the order of 38.4Å for the TSLS(mont), 34.2Å for the TSLS(Ce^{3+}-mont), 39.7Å for the TSLS(beid) and 38.7Å for the TSLS(Ce^{3+}-beid). These values are all reasonable for the pillared products based on the van der waals radius of imogolite (23Å) and the thickness of a clay layer (9.6Å). The relatively high surface areas of the TSLS complexes (approx. 300 m^2/g) indicate that these materials are indeed pillared and, as was previously described, the majority ofthe surface area is attributed to the internal channels of the imogolite tubes.

The presence of Bronsted acidity has been demonstrated by FTIR spectra of pyridine adsorbed on the surfaces of the TSLS complexes. Further evidence for the presence of Bronsted acidity has been shown by the catalytic cracking of

cumene to benzene in which the TSLS(beid) was the superior catalyst of the TSLS complexes tested.

The TSLS(beid) yielded significantly higher selectivity for m-xylene isomerization than the other TSLS complexes. The TSLS(beid) gave selectivities to isomerized products of nearly 90% while the other TSLS complexes were only near 50%. This is consistent with the increased Bronsted acidity of the TSLS(beid).

Decane cracking was substantial for the TSLS(beid) and very poor for the TSLS(mont) indicating that the number and strength of the acid sites is much higher in the TSLS(beid). The product distribution for decane cracking showed mainly C_4-C_6 products which is significantly different than that of even large pore zeolites in which C_3 and C_4 hydrocarbons are the main products.

TSLS(beid) was the best catalyst in regard to conversion, selectivity and deactivation of all of the catalysts tested. The thermal stability of the TSLS(beid) is at least as good as the TSLS(mont) and possibly better. Further investigation into pore sizes and thermal stability of the TSLS(beid) complex is suggested by these results.

LIST OF REFERENCES

1. Vaughn, D.E.W.; Lussier, R.J. Preprints 5th International Conference on Zeolites; Naples, Italy, June 2-6, 1980.

2. Pinnavaia, T.J. Science 1983, 220, 365.

3. Lahav, N.; Shani, V.; Shabtai, J. Clays Clay Miner. 1978, 26, 107.

4. Lopeppert, R.H., Jr.; Morland, M.M.; Pinnavaia, T.J. Clays Clay Miner. 1979, 27, 201.

5. Yamanaka, S.; Brindley, G.W. Clays Clay Miner. 1979, 27, 119.

6. Sterte, J.; Otterstedt, J. Applied Cat. 1988, 38, 131.

7. Adams, J.M. Applied Clay Science 1987, 2, 309.

8. Tilak, D.; Tennkoon, B.; Jones, W.; Thomas, J.M. J.Chem.Soc.,Faraday Trans. 1986, 82, 3081.

9. Barrer, R.M. "Zeolites and Clay Minerals as Sorbents and Molecular Sieves." Academic Press: New York, 1978.

10. Johnson, I.J., Werpy, T.A., Pinnavaia, T.J. J.Am. Chem. Soc. 1988, 110, 8545.

11. Corma, A.; Wojciechowski, B.W. Catal. Rev. Sci. Eng. 1985, 27, 29-150.

12. Ibid.

13. Plee, D.; Borg, F.; Gatineau, L.; Fripiat, J.J. J. Am. Chem. Soc. 1985, 107, 2362.

14. Pinnavaia, T.J., Landau, S. J.Mol. Cat. 1984, 27, 195-212.

15. Parry, E.P. J. Catal. 1963, 2, 371.

16. Vedrine, J.C.; et al. <u>J. Catal.</u> **1979**, *59*, 248.

17. Schutz, A.; Plee, D.; Borg, J.; Jacobs, P.; Poncelet, G.; Fripiat, J.J. Proceedings of the International Clay Conference, Denver, **1985**, 305-310.

18. Ocelli, M.L.; Tindwa, R.M. <u>Clays and Clay Miner.</u> **1983**, *31*, 22-28.

19. Mirodatos, C.; Barthomeuf, D. <u>J.Catal.</u> **1988**, *114*, 121-135.